

Copyright
by
Phil Jack Holzmeister
2010

The Thesis Committee for Phil Jack Holzmeister
Certifies that this is the approved version of the following thesis:

**Probing the coupling mechanism of opposite polarity
motors**

APPROVED BY

SUPERVISING COMMITTEE:

George Shubeita, Supervisor

Ernst-Ludwig Florin

**Probing the coupling mechanism of opposite polarity
motors**

by

Phil Jack Holzmeister

THESIS

Presented to the Faculty of the Graduate School of
The University of Texas at Austin
in Partial Fulfillment
of the Requirements
for the Degree of

MASTER OF ARTS

THE UNIVERSITY OF TEXAS AT AUSTIN

August 2010

Acknowledgments

I would like to thank my advisor, Dr. George T. Shubeita, for his guidance and help as well as for his constructive criticism throughout the last year. I would also like to thank Dr. Ernst-Ludwig Florin for taking the time to serve as a reader on my graduation committee.

I wish to thank my fellow PhD students Christina Leidel and Rafael Longoria for their support especially during the last weeks.

I want to thank the University of Würzburg and Dr. Fink from UT Austin for making this work possible during an exchange program.

Moreover, I wish to thank the Stiftung der Deutschen Wirtschaft (Foundation of German Business) for financial and non-material support throughout the past two years.

Last, but not least, I want to thank my parents for the last 24 years.

Probing the coupling mechanism of opposite polarity motors

Phil Jack Holzmeister, M.A.
The University of Texas at Austin, 2010

Supervisor: George Shubeita

Molecular motors are responsible for all long range transport and organization of organelles within cells. However, little is known about the interaction of multiple similar and dissimilar motors. In this thesis I describe experiments to probe the coordination of the motors kinesin and dynein which move towards the opposite ends of microtubules. Cargos they haul show bidirectional movement at short scales yet there is net transport in one direction or the other. Two distinct models for the bidirectional transport exist: regulation and a tug-of-war. In order to differentiate between them, kinesin-specific antibodies are injected into *Drosophila* embryos and the effect on transport of lipid droplets is quantified and compared to unperturbed motion. The function-blocking antibodies resulted in an increased run length of dynein-mediated transport and a decrease in that of kinesin. Furthermore, reduced velocities in both directions and a trend towards shorter pauses were observed. Comparison of these results to predictions the models provide for this scenario supports a tug-of-war model rather than regulation.

Table of Contents

Acknowledgments	iv
Abstract	v
List of Tables	viii
List of Figures	ix
Chapter 1. Introduction	1
Chapter 2. Background on molecular motors	3
2.1 Overview of molecular motors	3
2.2 Microtubules	4
2.3 Kinesin	5
2.4 Dynein	7
Chapter 3. Bidirectional transport - models and predictions	9
3.1 Regulation model	10
3.2 Tug-of-war model	12
3.3 Implications of differences between the two models	16
3.4 The advantage of antibodies over genetics	19
Chapter 4. Methods	21
4.1 The model system	21
4.1.1 The organism: <i>Drosophila melanogaster</i>	21
4.1.2 The cargo: Lipid droplets	22
4.2 DIC microscope and video recording	23
4.3 Sample preparation - reference data	26
4.4 Injection	28

4.4.1	Antibody preparation	28
4.4.2	Microinjection system	28
4.4.3	Micropipette preparation	29
4.4.4	Sample preparation - injected embryos	32
4.4.5	Injection of food coloring	34
4.5	Analysis	35
4.5.1	Tracking droplets	35
4.5.2	Analyzing tracks	38
Chapter 5.	Results	42
5.1	Reference Data	42
5.1.1	Run length distributions	43
5.1.2	Pause durations	47
5.1.3	Pause frequency	50
5.1.4	Velocity distributions	52
5.2	Effect of injection of anti- <i>Kinesin</i> antibodies	55
5.2.1	Injection of antibodies - large scale	55
5.2.2	Injection of antibodies - single droplet scale	56
5.3	Transport characteristics of embryos injected with antibodies	59
5.3.1	Run lengths	59
5.3.2	Pause durations	62
5.3.3	Pause frequency	63
5.3.4	Velocity distributions	65
5.4	Discussion	67
5.4.1	Comparison to <i>regulation</i>	69
5.4.2	Comparison to <i>tug-of-war</i>	70
Chapter 6.	Conclusion and future work	73
6.1	Summary and conclusion	73
6.2	Outlook	75
	Bibliography	77
	Vita	85

List of Tables

5.1	Runlengths in plus- and minus-direction for reference (OR-R), control (YW) and from [33]	47
5.2	Weighted mean velocities of droplet transport for reference measurements of Phase II embryos	55
5.3	Runlengths in plus- and minus-direction for samples injected with antibodies and comparison to the reference data	59
5.4	Weighted mean velocities of droplet transport for Phase II embryos after injection (velocity threshold $100 \frac{nm}{s}$). \bar{v}_R and \bar{v}_I are the weighted mean velocities for reference data and data after injections respectively	65

List of Figures

2.1	This drawing shows the two main players in our system: conventional kinesin (left) and cytoplasmic dynein (right). Both share similarities, like the two microtubule binding domains (heads), a cargo binding site and a motor domain that allows them to walk step by step. But dynein can only walk towards the minus-end of microtubules, whereas kinesin unidirectionally walks towards the plus-end. Dynein's structure is more complex than Kinesin's and the motors also differ in the way their motor domains function. Picture from [45] with permission from Elsevier	6
3.1	Illustration of the regulation model. First, <i>kinesin</i> (purple) is active and carries the cargo towards the plus-end and <i>dynein</i> (green) is "off". After some signal (here blue) switches the direction of transport, <i>kinesin</i> is inactive, while <i>dynein</i> is engaged and walks towards the minus-end. In this scenario opposite polarity motors never fight. Only relevant proteins are shown for simplification. The illustration reflects the basic concept of this model rather than proposing an actual mechanism.	11
3.2	Examples for different possible configurations of a <i>tug-of-war</i> between two <i>kinesin</i> and two <i>dynein</i> motors. These result in plus- or minus-end motion (bottom and top respectively) or in a state with no motion (center) until one team of motors is detached. The black arrows represent the direction in which the motors are pulling while the red arrows indicate the direction of motion. For simplification, only the motors involved are shown, all other proteins attached to cargo or microtubules are left out.	14
4.1	Fluorescent images of the microtubule (green) and nuclei (blue) orientation in <i>Drosophila</i> used in this work. The nuclei are aligned at the periphery. Microtubules (green) grow from the centrosome (outer side of the nuclei) and point towards the center of the embryo (plus-end). Therefore transport towards the periphery is accomplished by dynein whereas inward transport is caused by kinesin. Image courtesy of Susan Tran and Michael Welte.	22

4.2	Developmental phases of a <i>drosophila</i> embryo showing changes in lipid droplet distribution. Within two hours post-fertilization of the egg, droplets move bidirectionally with no net transport (left, Phase I). During this phase the embryo is a syncytial blastoderm, which means all nuclei are contained in a common cytoplasm. Right before cellularization starts, the nuclei align at the periphery of the embryo and a net transport of lipid droplets towards the inside can be observed (center, Phase II). This leads to a cleared area at the periphery. Afterwards during gastrulation (right, Phase III) a net transport towards the periphery can be seen. The microtubule orientation from Phase II on can be seen in fig.4.1	23
4.3	This schematic shows the principle of <i>differential interference microscopy</i> (DIC). One beampath is drawn as an example to explain the idea: The light comes from the top and after a polarizer it passes through a Wollaston prism. Here the beam is split into two beams with perpendicular polarizations. These pass the sample with a small spacial offset and are reunited by another prism. Now they interfere and the different optical pathlengths result in an intensity difference.	25
4.4	This shows a dechorneated embryo squashed in a groove between two thin coverslips which are glued to the glass slide. The coverslip on top flattens the periphery which extends to the sides of the groove. In this area, good images of the cargos moved by molecular motors can be acquired.	27
4.5	Micromanipulator stage with a micropipette. The stage can be remotely controlled and the injection is executed under the microscope. The tubing on the back of the needle leads to the microinjector which controls the applied pressure.	30
4.6	The pipette puller (right) used to produce the needles for injections. While the filament in the center is heated the glass melts and the weight pulls the glass tube apart into two micropipettes. The resulting tips show variation in shape (left). The tip diameter is $< 10 \mu m$	31
4.7	Embryo injected with food coloring, illuminated from above (reflection). The dye distributed quickly in the area of injection, while the diffusion towards the other end was slow compared to the time scale we are interested in.	35
4.8	Embryo injected with food coloring, illuminated from below (transmission). This picture was taken ca. 15 minutes after injection and the dye has not yet reached the opposite side. It is important to note that antibodies are much larger molecules than food coloring molecules and are expected to diffuse less in the embryo.	36

4.9	Tracking window of the LabView program used to track lipid droplets. The red box is the area defined as a template to be used in the next frame to look for the droplet within the green box using cross correlation. The red line on the screen is the track our chosen cargo has gone through from the start of the tracking process on.	38
4.10	Position of the cargo on the screen determined by the tracking program (see 4.9).The green solid line represents the microtubule the motor is supposed to walk on and is obtained by a least square fit. Microtubules can be assumed to be straight in the range of some micrometers.	40
4.11	Position of cargo along the microtubule as a function of time. The graph is obtained by projection of the tracking data onto a linear microtubule (fig.4.10). The inset highlights an area, where the parsing by <i>Marathon</i> into segments of constant velocity can be seen.	41
5.1	Plus- and minus-run length distributions of the reference data from wildtype <i>Drosophila</i> embryos. Each histogram was fit with a double exponential decay. The plus-end fit parameters were $D_{1+} = 701 \text{ nm}$ and $D_{2+} = 124 \text{ nm}$ with a reduced χ^2 value of 0.84 (top). Fitting the minus-runs (bottom) resulted in $D_{1-} = 495 \text{ nm}$ and $D_{2+} = 112 \text{ nm}$ at $\chi^2 = 1.75$	44
5.2	Plus-end run length distributions of the reference data from wildtype <i>Drosophila</i> embryos on logarithmic scale. It shows the same fit as in 5.1. As exponentials appear linear in this scaling, one can see that the data is well fit by the sum of two exponentials.	45
5.3	Pause durations for the reference data. The pause durations were fit by a single exponential decay. The fit resulted in a decay constant $\tau_{ALL} = 0.49 \text{ s}$ with $\chi^2 = 3.12$. Fitting only for pauses $> 0.75 \text{ s}$ improves the fitting quality to $\chi^2 = 1.04$ and gives $\tau_R = 0.61 \text{ s}$. The bins start at 0.25 s because this is our threshold for pauses.	48
5.4	The relative number of runs as a percentage of the total number of runs ($n = 4842$) are split for the different velocity ranges shown. 30.5% of the runs are pauses and the ratio between plus- and minus-end runs is $\frac{N_+}{N_-} = 1.04$. Runs with velocities between $50 \frac{\text{nm}}{\text{s}}$ and $100 \frac{\text{nm}}{\text{s}}$ are not used for the analysis of run lengths, given that they can be due to artifacts other than motor-driven transport. Their relatively small number and equal distribution between the opposite directions justifies their omission.	51

5.5	Histograms of the velocity distribution of runs ($> 100 \frac{nm}{s}$) for plus- and minus-end transport during Phase II. The mean velocities weighted by their duration are $\bar{v}_+ = 341 \pm 9 \frac{nm}{s}$ and $\bar{v}_- = 349 \pm 10 \frac{nm}{s}$	54
5.6	Development of an Embryo injected with antibodies against kinesin. In the area of injection (right side) lipid droplets have been transported to the outside of the embryo making it appear cloudy (dark) while the periphery on the opposite side still remains clear. Indicated times are times post-injection.	56
5.7	Image of an embryo injected with antibodies against <i>Kinesin</i> after recording the high magnification images. The reclouding is only local and less strong than for the example in fig.5.6. The reason for this is most likely leaking out of antibody solution due to squashing the embryo between the coverslip and glass slide for imaging. For many embryos, the reclouded area was even smaller.	57
5.8	Picture from a Phase II video of lipid droplet transport in the periphery of a <i>Drosophila</i> embryo injected with anti- <i>Kinesin</i> antibodies. Unlike embryos that were not injected with antibodies (fig.4.9), the field of view is already crowded with lipid droplets, implying biased transport towards the minus-end (top right). The purple lines represent the tracks obtained from this video. The residual transport in the plus-end direction (bottom left) indicates that not all <i>Kinesin</i> molecules were blocked. Nevertheless, global transport is obviously favoring <i>Dynein</i>	58
5.9	Plus- and minus-end run length distributions of lipid droplets after injection. Double exponential fits resulted in decay lengths of $D_{1+} = 312 nm$ and $D_{2+} = 57 nm$ with a χ^2 value of 0.77 for plus-end runs (top). The results for minus-runs (bottom) are $D_{1-} = 608 nm$ and $D_{2-} = 82 nm$ at $\chi^2 = 0.86$	60
5.10	The pause durations of the lipid droplet tracks after injection of the antibody were fit again to a single exponential decay. A pause duration of $\tau_{ALL} = 0.46 s$ with $\chi^2 = 1.07$ was obtained for the whole range and $\tau_I = 0.46 s$ with $\chi^2 = 0.82$ for fitting pauses longer than 0.75 s.	62
5.11	Relative number of runs in different velocity ranges compared to the total number of runs ($n = 2253$) after injection of antibodies. 28.8% of the runs are pauses and the ratio between plus- and minus-runs is $\frac{N_+}{N_-} = 1.04$. There are no obvious changes in this graph compared to the one obtained from reference data (see fig.5.4	64

5.12	Histograms of velocities of runs ($> 100\frac{nm}{s}$) for plus- and minus-end transport during Phase II after injection of antibodies. . . .	66
------	---	----

Chapter 1

Introduction

One of the most remarkable abilities of cells is to precisely localize organelles in the cytoplasm to where they are needed in a timely fashion. Simple diffusion of these cargos would lead to an even distribution over the whole cell. To achieve local differences in concentrations, cells make use of their transport machines - molecular motors (see 2) - which are proteins that transport cargo along the cytoskeleton, its filament infrastructure. This transport is directed and also has the advantage that it is faster than diffusion for long range transport. While the root mean square displacement (RMSD) $\sqrt{\langle x^2 \rangle}$ of diffusion is proportional to \sqrt{t} , the RMSD for transport by motor proteins is linear in time. Perhaps the most impressive example of this fast and directed motion occurs in melanophores. These are skin pigment cells possessed by some animals that enable them to quickly change their color from dark to light. To accomplish this, a melanophore uses molecular motors to aggregate its melanin-filled pigment granules in the center and therefore appear transparent within minutes. This transport is reversible and allows the cell to redisperse the granules and turn black again [15]

Among the various molecular motors (reviewed in the next chapter), the

ones that are relevant to this work are kinesin and dynein. These two motors move unidirectionally towards the opposite ends of microtubules. However, in many different systems, individual cargos are observed to move bidirectionally along these filaments, meaning that both types of motor contribute to their motion. Nevertheless, this back-and-forth movement is biased in one or the other direction in order to achieve a large scale trend in directionality of transport like in the melanophores mentioned before. The big question addressed in this work is how cells are able to achieve directed net large scale motion despite the fact that all individual cargos experience bidirectional movement.

At present, there exist two fundamentally different models to explain this behavior (see 3). One model, *regulation*, relies on a third party - a chemical switch - responsible for changing directions. Thus, only one type of motor is engaged at a time. The other model assumes that the opposite polarity motors stochastically engage in a *tug-of-war* and that the overall outcome of this fight is determined only by the properties of the motors and small changes to these properties. The models will be explained in more detail later with emphasis on their differences. My goal, as detailed in this work, is to create an experiment that is able to distinguish between these models. My approach is to perturb the transport system *in vivo* by disabling one type of motor on demand, and use the fact that the two models provide different predictions for such a perturbation.

Chapter 2

Background on molecular motors

2.1 Overview of molecular motors

Molecular motors are special proteins which fulfill various tasks inside a cell. Despite being different in their purposes and abilities, they all share one property: they are able to convert chemical energy, usually in form of ATP (Adenosine Triphosphate), into mechanical work. The specific motor structure determines the way this happens and allows classification into three groups of molecular motors.

First, there are the rotary motors like the one that propells the flagella of bacteria, thus enabling them to swim. Another example is the F_0F_1 -ATP *Synthase*, a motor present in the membrane of our mitochondria which works the other way around - driven by a proton gradient across the membrane, it rotates and synthesizes ATP in the process. It is noteworthy that this class of motors look and work quite similar to rotary motors invented by mankind, consisting of a rotor and a stator.

The second class of motors are the nucleic acid motors. Among them are *Helicases* which separate DNA strands before transcription or replication. Transcription and translation, in turn, are accomplished by *RNA polymerase*

and *DNA polymerase* by translocating along the nucleic acid strand. Therefore, the usage and storing of genetic information would not be possible without these proteins.

The last major group of motors are processive motors, which literally walk on the cytoskeleton of the cell. Members of the *Myosin*-family walk on actin filaments and are responsible for, amongst other things, muscle contraction. The *Kinesin* and *Dynein* families move on microtubules and as mentioned earlier, transport different types of cargos to their destination. In the next section I will review *Kinesin-1*, *Cytoplasmic Dynein* (see fig.2.1) and microtubules in more detail since these proteins play a central role in my thesis.

2.2 Microtubules

Microtubules, a major part of the cell's cytoskeleton, are tube-like filaments with a diameter of 25 *nm* and lengths ranging from hundreds of nanometers to tens of micrometers. They are formed by heterodimers consisting of α - and β -tubulin. Those polymerize into linear protofilaments and 13 of these, aligned side by side, form a hollow cylinder, the microtubule. Due to their heterodimeric nature, microtubules have a built-in polarity detectable at every point along their length and it is this polarity that defines the direction in which a certain motor can proceed. In the cell, the fast outward growing end is named the *plus-end*, while the other end at the center of the cell (at the centrosome from which they emerge) is called the *minus-end*. Knowledge of the orientation of microtubules in the system being studied is important because

each type of motor is only able to walk unidirectionally along the microtubule. I will describe the microtubule orientation in my model system in 4.1.1.

2.3 Kinesin

Conventional Kinesin, or *Kinesin-1*, was first discovered in 1985 in giant squid axoplasm [46] and has been recently identified as the plus-end motor for lipid droplets in *Drosophila* [38], the model system in my experiments (see 4.1). It is responsible for the majority of long-range transport in living cells. It is a heterotetramer, consisting of two heavy chains (KHCs) and two light chains (KLCs) with a total molecular weight of $\sim 380 \text{ kDa}$ [19]. The heavy chains form a dimer via a coiled coil (stalk) and contain the motor domain, including the so called heads, which bind to the microtubule. The light chains are the binding sites for various types of cargos (see fig.2.1).

Kinesin walks along the microtubule in a *hand-over-hand* mechanism, alternating the front head, like humans walk (“head” \rightarrow foot) [3]. One head is always attached to the microtubule and for each step one molecule of ATP is hydrolyzed [13]. With each step, the moving head proceeds about 16 nm (~ 2 tubulin dimers), resulting in an 8 nm displacement for the center of mass, which corresponds to the length of one tubulin dimer [52]. The motor is highly processive *in vitro*, moving cargos about 1000 nm before detaching from the microtubule [43] and, therefore, taking more than 100 steps on average. It moves at a velocity of $\sim 600 \frac{\text{nm}}{\text{s}}$ at saturated ATP level [22] and is able to exert a force of $\sim 5 \text{ pN}$ [47]. Two motors or more more of the same type

on one cargo increase the processivity significantly ($> 8 \mu m$) [47], but do not influence the velocity unless opposing load is significant [20].

It has to be noted that velocities, run lengths and forces are usually different *in vivo* due to the environment. The processivity is reduced by obstacles on microtubules [41] and there are of course opposite polarity motors present. Moreover, *in vivo* motor properties are likely modulated by motor regulators. In addition, characteristics like run length vary not only between different cell types, but also between different developmental phases *in vivo*. Values relevant for my work are mentioned later and compared to my data.

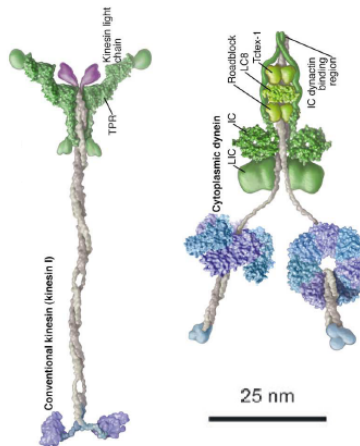


Figure 2.1: This drawing shows the two main players in our system: conventional kinesin (left) and cytoplasmic dynein (right). Both share similarities, like the two microtubule binding domains (heads), a cargo binding site and a motor domain that allows them to walk step by step. But dynein can only walk towards the minus-end of microtubules, whereas kinesin unidirectionally walks towards the plus-end. Dynein's structure is more complex than Kinesin's and the motors also differ in the way their motor domains function. Picture from [45] with permission from Elsevier

2.4 Dynein

Cytoplasmic Dynein, even though discovered around the same time (1987, [32]), is not as well-studied as *Kinesin-1*. It is a bigger protein, consisting of two 530 *kDa* heavy chains (DHCs), three intermediate chains and four light intermediate chains, adding up to about 1.2 *MDa* [19]. The basic layout - a cargo binding site, two heads, coiled coil in between - is similar to *Kinesin*, but at a closer look the motor domain in particular differs significantly. It is made out of a ring with 6 AAA^+ ATPase-like domains [35] and the microtubule binding site is located further away from the ATPase.

This motor also walks in *hand-over-hand* fashion [44], but the step size is not fixed as it is for *Kinesin*. *Dynein* seems to be capable of varying its stepsize between 8 – 32 *nm* depending on the applied load [26], which is comparable to switching gears in your car for driving uphill. Due to its long “legs”, *Dynein* is also more likely to switch between protofilaments and nearby microtubules. Similar to *Kinesin*, the processivity can be drastically increased if more than one *Dynein* is present [27]. However, unlike kinesin, the force dynein can exert is still a controversial issue. Reported values range from 1.1 *pN* [26] to ~ 7 *pN* [44] *in vitro* and from 1.1 *pN* [51] to 2.4 *pN* [38] and 3 – 5 *pN* [39] *in vivo*.

Dynein is typically associated with another protein cofactor which is able to bind to microtubules and cargos: *Dynactin*. If *Dynactin*, which does not cause motion on its own, is present *in vitro*, *Dynein* processivity is increased from 0.7 μm to 1.5 μm , while the velocity does not change (700 $\frac{nm}{s}$)

[21].

This all goes to show that a great deal of information has been gathered for single and multiple motors of the same type *in vitro*. However, the actual cellular environment is not as simple as *in vitro* experiments and this results in differences between values obtained *in vivo* and *in vitro*. As both plus- and minus-end motors are present on cargos, we are left with the question of how this complex intracellular transport is coordinated. The next chapter will therefore focus on which models exist to explain the observed transport and their predictions.

Chapter 3

Bidirectional transport - models and predictions

So far, a lot of protein cofactors (like Tau [47], BicD [24] or NudE [29]) that influence intracellular transport are known, but the coupling mechanism of opposite polarity molecular motors is not yet resolved. These motors, *Kinesin* and *Dynein*, transport cargos along microtubules, which are part of the cytoskeleton, and each can only walk specifically towards one end of the microtubule. So, in many different systems one can observe bidirectional transport along these filaments. All observed cargos like pigment granules in fish and frogs [1], secretory vesicles [49], lipid droplets in *Drosophila* [14], mitochondria [31] or mRNA [7] show a back-and-forth movement along microtubules. Despite this behavior, the cell manages to achieve net transport of the cargo to the place where it is supposed to be. Understanding the mechanism behind this has been investigated for years and, to date, there are two different approaches to explain the complex motion of cargos, a *tug-of-war* model and a regulation model. These models and evidence for them will be explained in the following. Differences between them and the way I want to benefit from these differences in my own experiment will be emphasized.

3.1 Regulation model

The regulation model explains the observed complex behavior with a third party which is responsible for switching directions and therefore coordinating transport. In this model, opposite polarity motors never interfere with each other, meaning there is a regulation complex which makes sure, that only one type of motor is engaged at a time. Thus, both *kinesin* and *dynein* are present on the cargo at all times, but when *kinesin* (*dynein*) is active, *dynein* (*kinesin*) is turned off. No matter how the regulation works in detail, the motors never fight against each other. In fact, there are obviously non-motor proteins affecting the transport, like dynactin (see 2.4). This candidate is able to bind to microtubules and cargos as well as to motors, thus increasing *dynein*'s processivity [21]. It has been shown that it also influences *kinesin* motion and can only bind to one motor at a time [11]. However, it has not been proven that it actively is responsible for switching the direction of motion. But discoveries like dynactin have led to a broad support of this model and some other indications are reviewed in the next paragraphs.

Gross et al. [16] also predicted a switch: the average run length of motors measured in *Drosophila* embryos, the same model system as used in this thesis (see 4.1.2), turned out to be significantly lower than the one observed *in vitro*. Especially if more than one motor is engaged, *in vitro* experiments show a processivity which is basically limited by the length of the microtubule [5]. Despite the fact that cargos carry several motors of the same type, runs of this length are rare *in vivo*, suggesting some control mechanism. Because

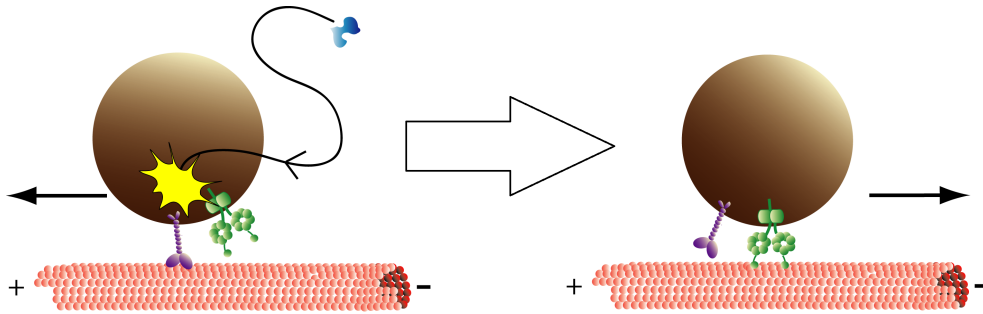


Figure 3.1: Illustration of the regulation model. First, *kinesin* (purple) is active and carries the cargo towards the plus-end and *dynein* (green) is “off”. After some signal (here blue) switches the direction of transport, *kinesin* is inactive, while *dynein* is engaged and walks towards the minus-end. In this scenario opposite polarity motors never fight. Only relevant proteins are shown for simplification. The illustration reflects the basic concept of this model rather than proposing an actual mechanism.

only a small part of their analyzed reversals ($\sim 13\%$) were associated with pauses, indicating immediate switching, they supported regulation rather than a *tug-of-war* situation. But as mentioned below, this behavior has now been reproduced using a *tug-of-war* simulation.

Another hint indicating a regulation model was found by reducing the expression of *kinesin* via mutations in *Drosophila* embryos. This did not only result in the expected decreased mean numbers of *kinesin* on cargos, but also decreased the number of engaged *dyneins* [38]. As it is hard to explain with a simple *tug-of-war*, this effect favors a regulation model and the authors suggested a model where opposite polarity motors can only attach to cargos in pairs. Even though this idea supports regulation, there is no direct proof that there is the same amount of *Kinesin* and *Dynein* present on the cargo.

They only determined the number of engaged motors with an optical trap. Moreover, a recent study [2] proposes a mechanism where opposite polarity motors engage each other mechanically which could explain the observations too (see 3.2).

In a different approach, Kural et al. [23] measured step sizes using fluorescent imaging with one nanometer accuracy (FIONA) of GFP-tagged peroxisomes in drosophila cells. In their opinion a *tug-of-war* situation, where motors walk into opposite directions and stretch, should displace the cargo in steps smaller than the usual 8 nm step size of motors. Because they report steps of the cargo of multiples of 8 nm , they discard a *tug-of-war* model. However, a look at the supplement data reveals that the stepsize distribution shows the claimed peaks at multiples of 8 nm - but also a significant amount of step sizes inbetween, especially around 0 nm . Even in a *tug-of-war* model, the normal motor step size is expected to be dominant. Only a small amount, during reversals or pauses, should show reduced steps. Therefore, they can not rule out a *tug-of-war* even with their own reasoning.

3.2 Tug-of-war model

The other possible way to explain bidirectional transport is the so called *tug-of-war*-model. The idea behind this model is that - like in the sport - you have two parties which try to pull in opposite directions. In the cell these two teams consist of *kinesin* motors trying to pull towards the plus-end of the microtubule and *dynein* motors trying to walk towards the minus-end.

Obviously the number of motors and the force they can exert are important factors which determine the winner of the fight. The detachment force and the so called binding and unbinding rates serve as analogs to the grip of the players in a *tug-of-war*. These describe the probability of the motors to attach to, or detach from, microtubules. It has been shown, that even small changes in these properties of the motors are able to explain the observed behavior [30]. These changes would still have to be arranged by a higher-order regulatory mechanism of the cell, but the transport itself directly involves nothing but the motors. The results include several motility states like fast plus- and minus-end motion as well as no motion or switching with and without interspersed pauses. (see fig.3.2).

The authors from the Lipowsky group modeled experimental data of motor-driven lipid droplets in drosophila embryos. By fitting their parameters to velocities, runlengths and stall forces for plus- and minus-end transport as well as to pause durations, they obtained values of their parameters (stall force, detachment force, binding rate, unbinding rate, forward and backward velocity) that were in accordance to reported experimental results. If there are more than just one or two motors on each side involved, it first sounds unlikely that one team is completely detached and therefore enables the other team to walk. To resolve this, they assumed an exponential increase of the unbinding rate with increased load force (Bell model [4]). Therefore, as soon as one motor is detached, the load force exerted by the opposite team increases per motor, thus resulting in a cascade of detaching motors. However, even

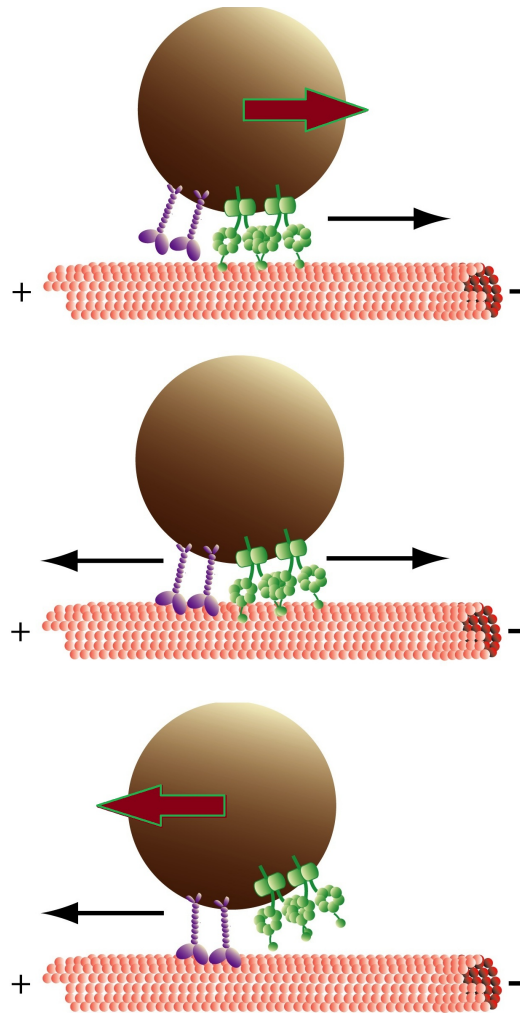


Figure 3.2: Examples for different possible configurations of a *tug-of-war* between two *kinesin* and two *dynein* motors. These result in plus- or minus-end motion (bottom and top respectively) or in a state with no motion (center) until one team of motors is detached. The black arrows represent the direction in which the motors are pulling while the red arrows indicate the direction of motion. For simplification, only the motors involved are shown, all other proteins attached to cargo or microtubules are left out.

if this idea is intuitive, it is lacking experimental proof and a similar motor, *Myosin*, has shown catch bond behavior [17], which means the lifetime of the motor-filament complex increases with applied load. They also approximated a linear force-velocity relation, where measurements have shown a different relation [48]. Moreover, there have been different experimental values reported since, for example for the stall-forces (see 2). But despite all of this, their work demonstrated that a *tug-of-war* model is basically capable of explaining bidirectional motion.

Recently Ally et al. [2] showed that transport *in vivo* needs both polarity motors to work. They replaced one motor with a substitute for which they tuned its ability to bind to microtubules, the cargo and to hydrolyse ATP. Motion in one or the other direction was only observed if the substitute was capable of walking along microtubules, even though the unaltered motor remained intact. This was the case for both *kinesin* and *dynein* replacements, suggesting that any pair of opposite polarity microtubule-based motors can activate each other. The mechanical interaction presumably necessary for activation of the motors seems to support a *tug-of-war* model. But as an opposite polarity motor is not necessary *in vitro*, these results are not completely conclusive and could also speak for regulation *in vivo*.

Further indication for a *tug-of-war* model was found by Soppina et al. [40] by discovering stretching of endosomes in *Dyctostelium* cells during reversals. Combining this and a signature of motion during reversals with force measurements *in vitro*, they assume a *tug-of-war* between one strong *kinesin*

and multiple weaker *dyneins*. However, as they are not sure about the actual microtubule orientation *in vivo*, they could only ascribe motion to the motors *in vitro* using polarity labeled microtubules in a 200-fold diluted cell extract, which might possibly have affected a regulatory complex. Furthermore only 32% of the observed tracks showed reversals at all and most of the remaining tracks were runs towards the minus-end (81%). It is likely, then, that endosomes *in vivo* are transported by *Dynein*, and reversals *in vitro* are due to spurious attachment of *kinesin*. This would lead to vesicle stretching due to an imposed *tug-of-war*. Transport of these vesicles is different than typical bidirectional transport of other cargos that reverse direction often. Thus, the mechanisms that govern motor coupling are likely to diverge between these systems.

3.3 Implications of differences between the two models

There are two main differences between these two models. One is that the regulation model implies a direct involvement of a third player while for the *tug-of-war* model variability of the properties of opposite polarity motors is sufficient. This means that a higher order regulation mechanism, which is mandatory for both models as the observed behavior changes over time, targets either a coordination complex or the properties of the motors directly. This can be used to probe the models by purifying cargos with motors from the system and transferring them into an *in vitro* environment, where all the additional components of the cytoplasm, and therefore the proposed regulatory

complex should be missing.

Such an experiment has recently been reported by Hendricks et al. [18]. The authors were able to reproduce the run length distribution observed in neurons with purified vesicles *in vitro*. Run lengths are defined as continuous motion in one direction until a reversal or pause occurs and their distributions usually differ between plus- and minus-motion [14]. However, their published data does not distinguish between directions. Nevertheless, the relative amount of long runs and the ratio between plus- and minus-end motion appear to be close to the *in vivo* results, which supports the idea of a *tug-of-war*. A similar experiment is currently underway in our group, while my approach targets the other main difference between the models described next.

In the *tug-of-war* model, *kinesin* and *dynein* are trying to walk all the time and therefore fight against each other as soon as both types of motors are attached to the microtubule. Contrary to this a regulation model simply switches between plus- and minus-end motion - without having them fight. With this information one can start and make predictions about how cargo is transported when one type of motor is inhibited from attaching to microtubules.

The two models predict different outcomes if one motor is removed from our system. Looking at the mechanism of a *tug-of-war* model we will expect longer runs of the remaining motor as runs should be limited only by the processivity of the motor which can be significantly larger than usually

observed *in vivo* (see 3.1). Unlike in the setup with both motors there should be nothing stopping the movement unless the cargo gets stuck in the cytoplasm or the motor detaches by chance - still, the average length of runs will increase. Hand in hand with longer duration of runs might go a decreased pause frequency and we can also expect pauses, if caused by a *tug-of-war*, to be resolved faster.

For a regulated transport we would not expect a significant change in the length of runs and in the pause frequency. Because some regulatory complex will determine how often motion is switched between plus- and minus-end, removing one motor type will not affect the length of a single run in the other direction. But what happens after a switching signal is received and there is no motor to attach to the microtubule? It could either happen that the cargo detaches and diffuses away or the cargo can pause at its position until the next switching occurs. Neither would change run length distributions, but the latter would increase pause durations. The last scenario is not unlikely considering dynactin is present and can bind both to cargos and microtubules [36], therefore keeping cargos in place without motors attached to microtubules.

If it is not possible to remove all motors of one type, but only some of them, one should still be able to detect these trends. In summary, increased run lengths will support a *tug-of-war* model, while increased pause durations of the transport will speak for a regulation model.

3.4 The advantage of antibodies over genetics

Getting rid of one motor type can be achieved in two different ways. In most cases so far, studies involved genetics as can be seen in some of the examples above. Genetically altering one of the motors, be it either to make it completely dysfunctional or just reduce its ability to walk, suppressing its expression or replacing it with synthetically built motor proteins, all have a common problem: One can never be sure that an observed change in the transport characteristics can be ascribed solely to the altered motor as opposed to an indirect effect. It is often the case that the living cells compensate for the lack of one protein by altering the expression or association of another, making it difficult to tease out cause and result. This is especially the case in my experimental system where it has been shown that reducing expression of *Kinesin* simultaneously reduces *Dynein* association to the cargo [38]), making it difficult to draw conclusions.

The other possibility to take out one polarity motor is using function blocking antibodies. This way, the system is intact at the beginning and cells develop completely normally. Introducing antibodies can perturb the system and probe the predictions we made previously. For my experiment I injected function-blocking antibodies against the *kinesin* heavy chain (KHC) of *kinesin-1* in *Drosophila* embryos. I am interested in the change of transport characteristics of lipid droplets during a certain developmental phase, in which transport by *kinesin* usually outweighs the one by *dynein*. Comparing especially run length and velocity distributions, as well as pause durations to

the predictions stated above, will enable me to favor one of the two models presented in this chapter. More detailed information about the model system, sample preparation, experimental setup and analysis of the data will be provided in the following chapter.

Chapter 4

Methods

4.1 The model system

4.1.1 The organism: *Drosophila melanogaster*

The system I used to test motor coordination is *Drosophila melanogaster* (fruit fly). A big advantage of this species is that we already know its genome [12] and a lot of mutants that target certain genes are characterized. Further reasons for the popularity of *Drosophila* are a short life cycle (~ 10 days) and the small amount of effort it takes to maintain a large population. Our group specifically uses the embryos of the fruit fly as a model system for intracellular transport. Approximately two and a half hours after the egg is laid, the embryo enters a developmental phase where nuclei are aligned along the periphery prior to cellularization. Motor-driven cargo transport can be observed in the vicinity of the nuclei. In order to ascribe motion to kinesin or dynein we need to know the orientation of microtubules inside the embryo. It turns out that microtubules form a basket around the nuclei with the centrosome at the point closest to the periphery [50] (see fig.4.1). This is where the minus-ends assemble and the plus-ends of the microtubules point inwards and allows us to ascribe motion towards the outside(inside) to dynein(kinesin).

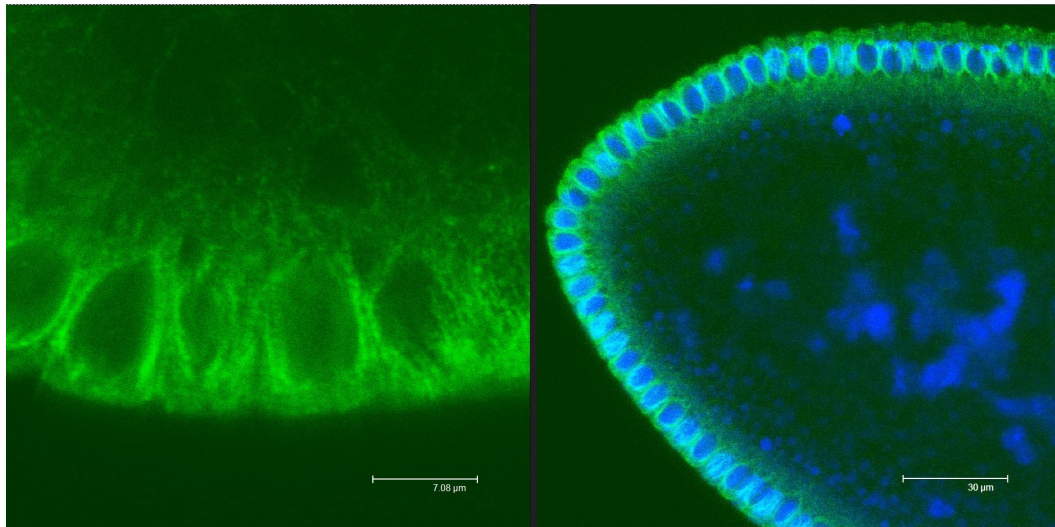


Figure 4.1: Fluorescent images of the microtubule (green) and nuclei (blue) orientation in *Drosophila* used in this work. The nuclei are aligned at the periphery. Microtubules (green) grow from the centrosome (outer side of the nuclei) and point towards the center of the embryo (plus-end). Therefore transport towards the periphery is accomplished by dynein whereas inward transport is caused by kinesin. Image courtesy of Susan Tran and Michael Welte.

4.1.2 The cargo: Lipid droplets

The cargo we use to characterize transport are lipid droplets which are spherical agglomerates of lipids inside the embryo. Before the embryo enters the developmental phase described above, these droplets are distributed everywhere in the vicinity of nuclei. Bidirectional motion along microtubules already exists, but there is no net transport (Phase I [51]). Consequently, during the cellularization process, lipid droplets are transported into the center of the embryo. This Phase II is referred to as “clearing”, because the periphery

turns from opaque to transparent (fig. 4.2). This phase is useful for us because, due to the limited amount of lipid droplets present in this area, we are able to track single droplets. It is also helpful for better imaging in general and for force measurements using an optical trap. All of this would be much harder if it was more crowded. Later on in development, the lipid droplets distribute again all over the periphery which is the so called “clouding” or Phase III.



Figure 4.2: Developmental phases of a *drosophila* embryo showing changes in lipid droplet distribution. Within two hours post-fertilization of the egg, droplets move bidirectionally with no net transport (left, Phase I). During this phase the embryo is a syncytial blastoderm, which means all nuclei are contained in a common cytoplasm. Right before cellularization starts, the nuclei align at the periphery of the embryo and a net transport of lipid droplets towards the inside can be observed (center, Phase II). This leads to a cleared area at the periphery. Afterwards during gastrulation (right, Phase III) a net transport towards the periphery can be seen. The microtubule orientation from Phase II on can be seen in fig.4.1

4.2 DIC microscope and video recording

Differential interference contrast microscopy (DIC) is an optical microscopy contrast technique for transparent objects. The high contrast is achieved by splitting linear polarized light with a *Wollaston* prism into two or-

thogonally polarized, but mutually coherent beams and sending them through the sample with a small spatial offset. After the objective, the beams are reunited by a second *Wollaston* prism and interfere. Thus, there are basically two brightfield pictures interfering, but as both experience different optical pathlengths (index of refraction n times pathlength l) due to the offset, the phase at each point of the beams is slightly different. The interference results in a non-linear conversion of a phase difference into an intensity difference which gives us the image we can record. The principle of the DIC microscope is shown in fig.4.3. It can be easily shown, that a phase difference of $\Delta\Phi$ results in a intensity difference of $\Delta I(\Delta\Phi) = I_0(1 + \cos \Delta\Phi)$, meaning there should be phase difference of not more than π in order to get clear pictures. This makes it a suitable tool for imaging thin biological samples as there are only small changes in the index of refraction.

Being able to detect these small changes is a huge advantage as the differences of the index of refraction within the cell are only in the order of 0.1. Moreover, there is no need for staining the sample unlike with fluorescent microscopy, the other main microscopy technique used in imaging of biological samples. In order to achieve a high signal-to-noise-ratio, samples should be as thin as possible, because this reduces phase shifts due to layers above and below the focal plane which will decrease the clarity of the image. As mentioned above, our area of interest is mostly empty during phase II, resulting in a good contrast for the few lipid droplets present there.

The DIC Microscope used is a *Nikon TE2000-U* with a 100x Objec-

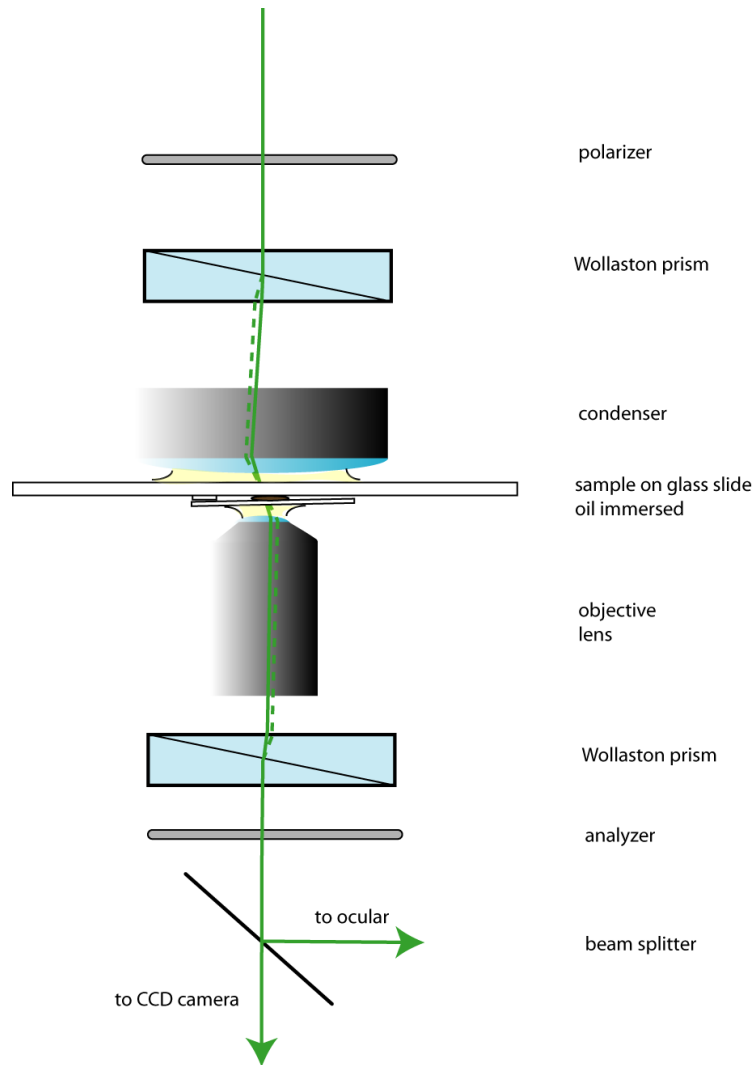


Figure 4.3: This schematic shows the principle of *differential interference microscopy* (DIC). One beampath is drawn as an example to explain the idea: The light comes from the top and after a polarizer it passes through a Wollaston prism. Here the beam is split into two beams with perpendicular polarizations. These pass the sample with a small spacial offset and are reunited by another prism. Now they interfere and the different optical pathlengths result in an intensity difference.

tive lens. Both condenser lens and objective lens use oil immersion for higher numerical aperture. Illumination is provided by a mercury lamp (*Nikon Intensilight C-HGFI*) and videos are recorded with a *DAGE-MTI CCD100* at 30 frames per second on VHS and afterwards digitized. The relation between actual distance and pixel size is determined with a ruler engraved on a glassslide (0.1 mm separated in 2 μm segments) to be 30.1 nm in x- and 30.3 nm in y-direction, where x represents the horizontal axis and y the vertical axis. This was achieved by taking snapshots of the ruler and determining the distance between maxima of greyscale values along a line of pixels.

4.3 Sample preparation - reference data

In order to collect useful *Drosophila* embryos, some hundred flies are collected in a plastic cup. The lid consists of a petri dish, filled with a mixture of agar, dextrose and apple-juice. By placing a small amount of yeast on this plate, the flies are triggered to lay eggs. Turning the cup upside down increases the amount of embryos placed on the lid and not somewhere else in the cup. The plate is exchanged by a new one after 2 1/2 hours, when the first embryos are at the age we are interested in, while eggs laid later will develop to this point during the next hours, which allows us to use one of these plates for ~ 2 1/2 hours. Embryos of the correct age are determined by eye under a *Nikon SMZ800* microscope (magnification up to 63x) after covering the plate with Halocarbon oil, which renders the embryo membranes translucent due to its high refractive index. The desired developmental phase (phase II) appears

as a clear periphery with elongated nuclei and a membrane growing into the embryo, visible as a thin line.

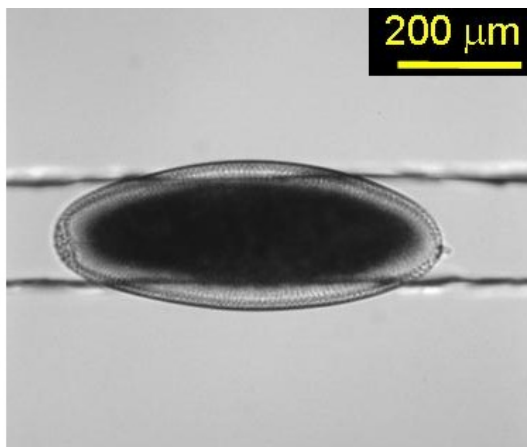


Figure 4.4: This shows a dechorneated embryo squashed in a groove between two thin coverslips which are glued to the glass slide. The coverslip on top flattens the periphery which extends to the sides of the groove. In this area, good images of the cargos moved by molecular motors can be acquired.

Once an embryo is found, it is prepared following the procedure described in [51]: using tweezers, the embryo is transferred onto double-sided tape and dechorneated (the chorion is removed). After this it is placed in a groove between two thin coverslips (Thermo Scientific No.0 thickness), which is just slightly thinner than the embryo. After placing a spacer of a glass coverslip on one side of the groove and covering the embryo with $\sim 20 \mu\text{l}$ of Halocarbon oil, another coverslip (Fisher Scientific, No.1 thickness) is put on top of the spacer and embryo. This pushes most of the embryo down in the groove, while the periphery is flattened out on both sides. Therefore, the area we are interested in, is well prepared for DIC microscopy, as the sample there

is transparent and thin.

4.4 Injection

4.4.1 Antibody preparation

The antibodies used for injection are *Cytoskeleton AKIN01* (rabbit polyclonal, anti-KHC), which identifies *Drosophila Kinesin-1* [34]. According to FRAP experiments (Fluorescent Recovery After Photobleaching) this antibody inhibits *Kinesin*-mediated transport in chicken dorsal root ganglia [42]. They were prepared following the description in previous papers [37] [38]. The antibody powder ($50 \mu\text{g}$) is suspended in $200 \mu\text{l}$ MilliQ water as instructed in the data sheet, which gives us an initial concentration of $250 \frac{\mu\text{g}}{\text{ml}}$. After dialyzing for 6 hours against 1l of 1x *PBS* in a *Slide-A-Lyzer Mini Dialysis Unit* (*Pierce, 10kDa MWCO*), the solution is concentrated using a *Amicon Ultra-0.5 mL Centrifugal Filter* (*Milipore, 30kDa NMWL*). The centrifuge settings for concentration are 1 hour at $14,000 \times g$, the concentrate is recovered afterwards from the filter by spinning for 2 minutes at $1,000 \times g$. All preparation steps are performed at 4°C . The final concentration of antibodies is $2 - 3 \frac{\mu\text{g}}{\mu\text{l}}$.

4.4.2 Microinjection system

The setup used for injections consists of a *Xeneworks Microinjector* and a *MP-285 Micromanipulator*, both from *Sutter Instruments*. While the manipulator is used to position the micropipette, the injector provides the pressure for the injection.

Consisting of 3 stepper motors, the micromanipulation stage can be used to move the micropipette in steps of down to $0.04 \frac{\mu m}{step}$ in X-, Y-, and Z-direction of a cartesian coordinate system, with X and Y on the base plane and Z perpendicular to it. For my purposes I defined a 4th axis to be able to inject from a 45-angle and penetrate the membrane more easily. The stepper motors are controlled with a remote control, which also allows to switch between fine and coarse movement as well as between the predefined 3 axis and the self-programmed 4th one. In addition to the range of 2.5 cm in each direction provided by the manipulator itself, I mounted it on a stage that I designed to allow more freedom in positioning the manipulator in all directions.

The second part of the injection system is the microinjector, which is able to apply pressure of up to 15 psi above and 7 psi below air pressure. The pressure output is attached with a plastic tube to the micropipette holder on the manipulator stage. Applied pressure is controlled with a remote, which enables us to not only apply static pressure, but also pulses. In addition to the gradually variable static pressure, one has the option to define an injection pressure. The solution is injected at this pressure as a pulse with adjustable pulse width ($0.01\text{ s} - 10\text{ s}$), or as long as the injection button (or foot pedal) is pressed.

4.4.3 Micropipette preparation

The last tool necessary for injection of the antibody solution, is a micropipette which can be moved by the micromanipulator stage and is con-

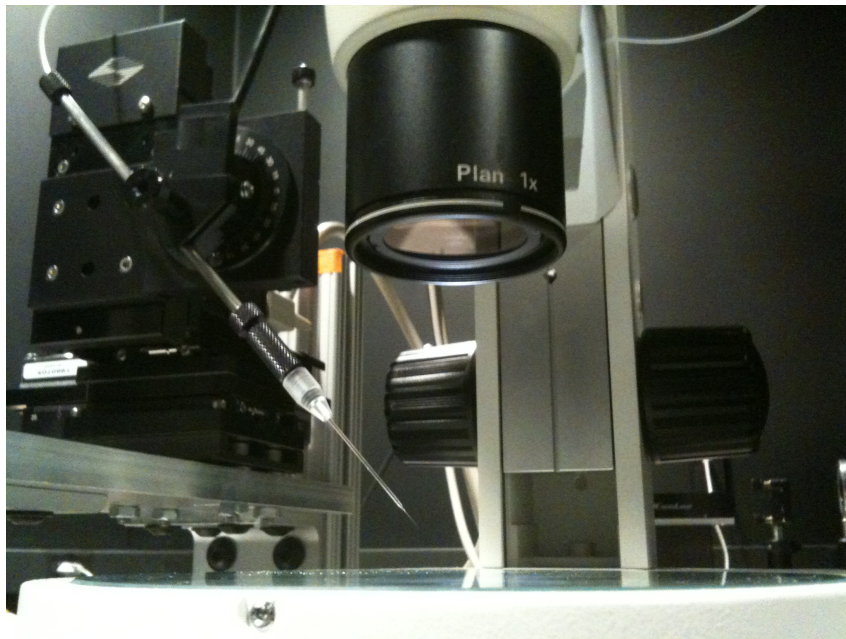


Figure 4.5: Micromanipulator stage with a micropipette. The stage can be remotely controlled and the injection is executed under the microscope. The tubing on the back of the needle leads to the microinjector which controls the applied pressure.

nected to the microinjector. The pipette is produced from borosilicate glass tubes (SUTTER, outer diameter: 1.0 mm, inner diameter 0.58 mm). The glass is vertically fixed in a needle puller (NARISHIGE PB-7, Stein lab in Patterson building), which basically consists of two clamps to attach the glass, a heating filament around the glass in the center and some weight on the lower end. As the pulling sequence is introduced the filament is heated in a predefined way (maximum temperature and pace of heating) and the weight pulls the lower part down, causing the glass tube to melt and rip apart. This results in two pipettes, but usually only the upper one shows a promising tip.

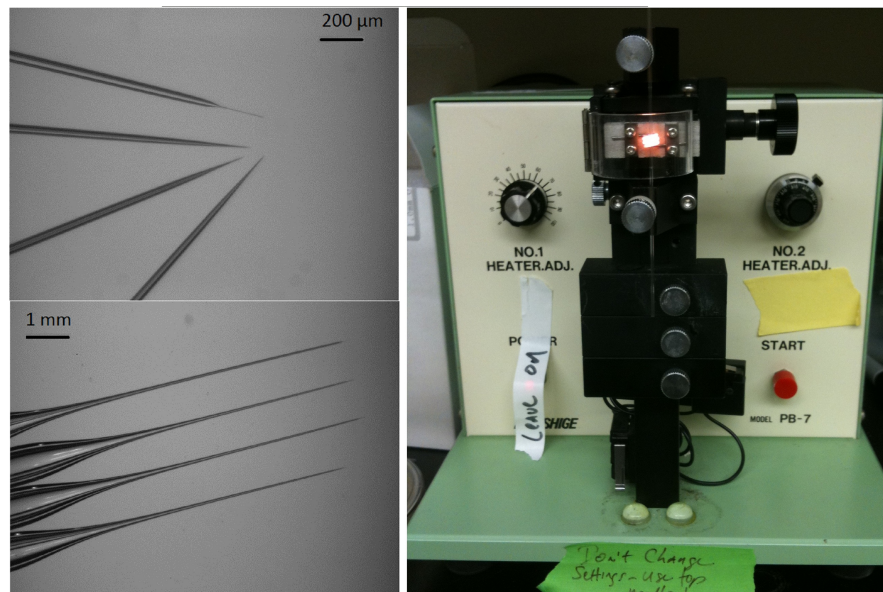


Figure 4.6: The pipette puller (right) used to produce the needles for injections. While the filament in the center is heated the glass melts and the weight pulls the glass tube apart into two micropipettes. The resulting tips show variation in shape (left). The tip diameter is $< 10 \mu\text{m}$.

Due to problems with their machine, the resulting tips were only to a certain extent reproducible and changed therefore in shape and diameter (see fig.4.6). But as the Stein group uses the pipettes for their work with *Drosophila*, their settings can be used for my experiment, too. After producing the pipette, the tip is usually still closed because of the melting process and needs to get broken manually. This is done right before it is used for injection to avoid getting dust in it. It can be broken under the microscope either by using a tweezer or a razorblade or by rubbing it on the edge of the glass slide using the micromanipulator. The resulting tip diameters are smaller than $10\ \mu m$.

4.4.4 Sample preparation - injected embryos

Up to the point of dechorneation, embryos are prepared similar to 4.3, but should be slightly younger in order to image them at the same age after a longer preparation procedure. To achieve this, embryos which already show the ingrowing membrane, but have it as close to the periphery as possible, are chosen. After dechorionating it, the embryo is placed on a glass slide without oil in order to dry and stick to the glass to facilitate injection. I found that ~ 7 minutes is a good compromise between too long exposure to a dry environment, which eventually damages the embryo, and too little time to stick, thus not providing enough resistance against the pressure of the injection pipette.

During this time, the micropipette can be prepared and loaded with antibody solution. The tip has to be broken as described above, followed by

filling the needle. The latter can be achieved in two ways. The pipette can either be loaded from the back or from the front. Back-loading provides an advantage, if many embryos have to be injected in a short amount of time. In my trials back-loading resulted in the formation of air bubbles close to the tip, which is undesirable. Moreover, due to remains from the embryo's cytoplasm, the tip was often clogged and therefore useless after one or two injections. Because of this, I preferred front-loading of small quantities, namely sucking in antibody solution from a small drop placed on the slide by applying negative pressure with the microinjector.

In order to get an idea of the ratio of antibodies to kinesin, we first need to know the volume of an embryo. According to [10], the average length and width are $400\ \mu m$ and $250\ \mu m$ respectively. Thus we can estimate a volume of less than $V_E = 25\ fl$. The concentration of kinesin has been determined in squid axoplasm to be $0.5\ \mu M$ [6]. The molar concentration of our antibody solution is $c_{mol} = \frac{c}{M_{AB}} = \frac{2g/l}{150\ kg/mol} = 13\ \mu M$ for a conservative estimation with low AB-concentration and a heavy antibody (the actual molecular weight is not provided by *Cytoskeleton*). The injected volume is estimated to be more than 1/20-th of the embryo volume, as dilution of the cytoplasm during injection is clearly visible in the injection area. Therefore, the molar concentration of antibodies ($\frac{13}{20}\ \mu M = 0.65\ \mu M$) is comparable to the concentration of *Kinesin*. Even if *Kinesin* is more abundant in our system, the fact that the antibodies mostly remain around the injection area, due to limited diffusion as can be seen in the next section (4.4.5), its local concentration will be higher than our

estimate.

After the *Drosophila* embryo has attached to the glass and the pipette is loaded, we lower the tip remotely with the manipulator stage until there is contact with the embryo. The continuously applied pressure should be ~ 0.8 psi (a value of 50-60 on the display) to equalize the pressure inside the embryo and prevent backflow of cytoplasm into the needle. Consequently, we switch to the diagonal axis of the manipulator and penetrate the embryo. The constant pressure is then increased until dilution of the cytoplasm is visible, indicating injection of the clear antibody solution. If this is not possible (due to clogging of the tip), the injection pressure pulse is used, starting with low pressures and increasing the settings until the effect occurs. Once this is done, the needle is removed from the embryo and the latter is covered with *Halocarbon oil 27* and a glass coverslip. The oil does not influence the further development of the embryo, but increases the resolution. The sample is now ready for the microscope.

4.4.5 Injection of food coloring

The injection of green food coloring is used as proof of principle for my injection technique. The dye used is food coloring diluted in water and injected into embryos of the age we are interested in. It can be seen that within seconds the area around the injection turns green, whereas the other end of the embryo remains unchanged (fig.4.7, 4.8). These pictures were taken with an iPhone through the ocular of the microscope as the attached camera only

records greyscale pictures. This accounts for the less-than-optimal quality of the image. Injecting food coloring was also used as a control to insure that there are no artifacts due to the injection process. Especially in fig.4.8 one can see that the injection itself does not cause reclouding of the lipid droplets, even though this picture was taken several minutes after the injection. Considering these pictures we can expect a significant difference in the environment of the motors in different parts of the embryo.



Figure 4.7: Embryo injected with food coloring, illuminated from above (reflection). The dye distributed quickly in the area of injection, while the diffusion towards the other end was slow compared to the time scale we are interested in.

4.5 Analysis

4.5.1 Tracking droplets

In order to quantify the motion of molecular motors from recorded videos, we need to track the lipid cargos which are transported by them. Considering their step-size (e.g. 8 nm for *Kinesin*, see 2), it is obvious that the precision of our tracking has to be in that range, too. Otherwise we might



Figure 4.8: Embryo injected with food coloring, illuminated from below (transmission). This picture was taken ca. 15 minutes after injection and the dye has not yet reached the opposite side. It is important to note that antibodies are much larger molecules than food coloring molecules and are expected to diffuse less in the embryo.

miss important information about the behavior of motors or might be led to wrong conclusions. To achieve precise cargo tracking I used an algorithm for single particle tracking based on cross-correlation combined with parabolic interpolation as detailed in [9] and briefly described below.

As mentioned earlier, the pixel size in our images corresponds to about 30 nm in the sample in the x- and y-directions. This would basically limit us to determine the position of cargos only in 30 nm jumps, which would not reflect the behaviour of motors. However, given that the lipid droplets have a diameter of several hundred nanometers and, therefore, span over ~ 10 - 15 pixels, we can use the information contained in that extended region to determine the center with a precision exceeding the pixel size. For that we use cross-correlation in order to get around the restrictions set by the pixel-size: our tracking program in LabView allows us to choose an area of interest and saves it as a template. It then compares consecutive frames within a certain

search area around our droplet and determines the position of the center of the best match to the template (see fig.4.9). Correlation works best for well-defined objects, which imposes criteria we have to consider when we choose the droplets we want to track.

One important aspect is of course, that the object changes its appearance as little as possible during the time we want to track it. Changes can occur due to motion in and out of focus. If the object changes appearance, the tracking program might simply not be able to follow the lipid droplet, or it could also determine the center of the template inaccurately. Another criterion is good contrast against the background. This obviously allows better tracking than if you have only a blurry image of your droplet. After tracking, one has to make sure that the track does not show pixel latching - repeated clustering of the tracked position with jumps equal to the pixel size inbetween - indicating bad tracking for reasons mentioned above.

In addition to these criteria concerning the imaging, there are some other important things to consider. Due to the orientation of microtubules in our experiment (see fig.4.1), only tracks from cargos moving along that direction can be analyzed as we cannot be sure of the microtubule polarity if the cargo moves in different directions. Cargos can only be tracked until they run into other droplets or until they leave the field of view or the area where microtubules are relatively straight. It does not make sense to track them in the bulk of the embryo or right at the periphery where microtubules are not oriented straight. Having these considerations in mind, we have to



Figure 4.9: Tracking window of the LabView program used to track lipid droplets. The red box is the area defined as a template to be used in the next frame to look for the droplet within the green box using cross correlation. The red line on the screen is the track our chosen cargo has gone through from the start of the tracking process on.

track everything else in order to get a representative picture of the transport characteristics. This guarantees unbiased results which can be undermined if only large droplets or long travellers are selected.

4.5.2 Analyzing tracks

Once the tracks are available as *.txt files of position and time, we use the program *Marathon* to split the tracks into segments of constant velocity.

The program is described in detail by Petrov et al.[33] and is available on the homepage of the group of Steve Gross (UC Irvine). Therefore, I will only give a short overview of how this process of parsing tracks works.

First, the program fits a linear microtubule to the data via linear regression. As the length of most tracks is in the order of some micrometers and considering the geometry (fig.4.1), microtubules can be approximated as straight filaments for this range. Subsequently, all data points are projected onto this line, resulting in a description of the cargo position along the microtubule as a function of time (fig.4.11). This projection is the best way we have to determine the motor position from the position of the cargo. As motors are almost 100 nm long and the diameter of lipid droplets is a few 100 nanometers, a displacement of the droplet center of around 200 nm perpendicular to the microtubule can be expected. If multiple motors as well as *Dynactin* are attached to the cargo and the microtubule, the displacement of the droplet in the direction of the microtubule can be expected to be smaller.

The program uses a *Bayesian* approach to split this new track into segments of constant velocity. It starts with a large number of small segments. Consecutive segments are then merged if in doing so the fit is affected the least. This process is continued till the fit quality exceeds what would be expected if one were to fit the position of a diffusing cargo that is tethered to the microtubule but not being transported.

This procedure results in tracks split into short segments, but we are mostly interested in properties of runs. A run in this context is defined as the

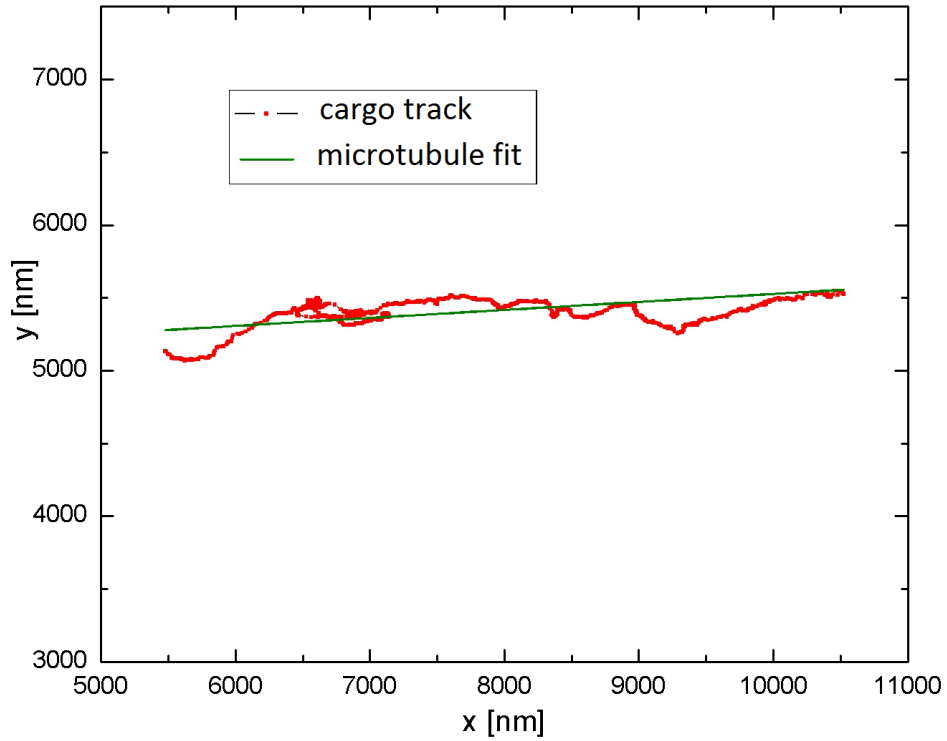


Figure 4.10: Position of the cargo on the screen determined by the tracking program (see 4.9). The green solid line represents the microtubule the motor is supposed to walk on and is obtained by a least square fit. Microtubules can be assumed to be straight in the range of some micrometers.

distance a cargo moves in one direction until it stops or reverses its motion. Therefore, a run can consist out of several segments with different velocities. Runs with velocities lower than $50 \frac{nm}{s}$ are considered pauses if they last for at least 7 consecutive frames ($\sim 0.23 s$). This velocity threshold is well below usual motor speeds of $> 100 \frac{nm}{s}$. To get a representative picture of the transport, the first and last run of each track are dropped. This way, personal bias in choosing droplets for tracking is reduced, because from the first pause or

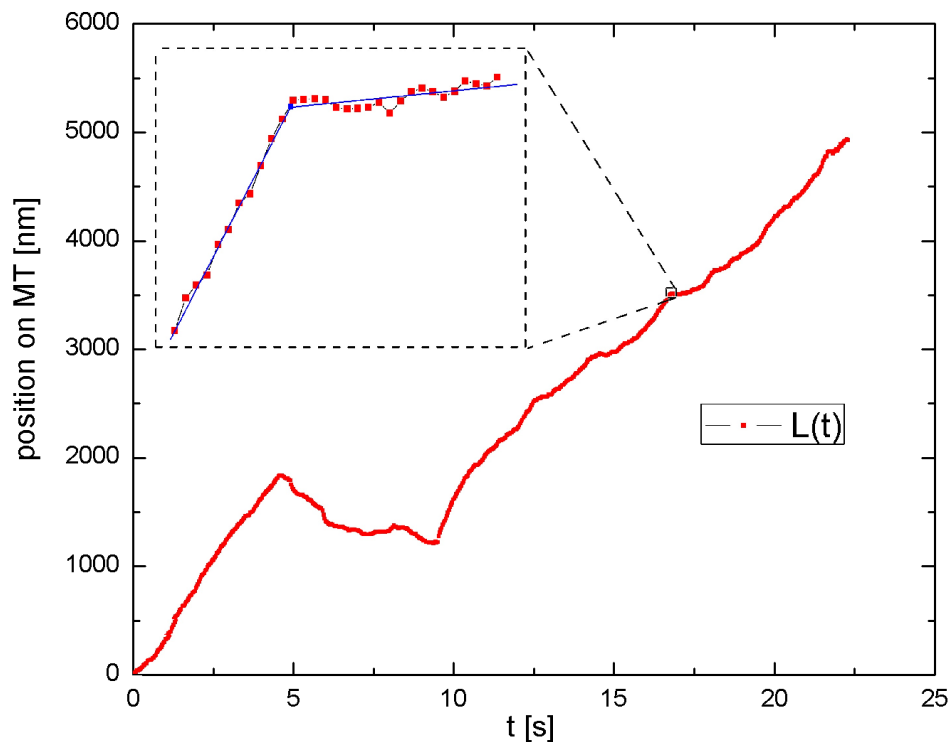


Figure 4.11: Position of cargo along the microtubule as a function of time. The graph is obtained by projection of the tracking data onto a linear microtubule (fig.4.10). The inset highlights an area, where the parsing by *Marathon* into segments of constant velocity can be seen.

reversal on, the behavior is supposed to be independent of the history of motion. We split our data into runs in the plus- and minus-direction and pauses and use these in our analysis.

Chapter 5

Results

In this chapter, I first analyze the characteristics of lipid droplet transport in my reference data consisting of wild-type embryos. I will then determine the same transport characteristics for the data I obtained from the embryos I injected with antibodies against *Kinesin* and identify changes. Subsequently, in the discussion section, I will compare these results with my predictions described in 3.3 for the models for bidirectional transport.

5.1 Reference Data

I used wildtype *Drosophila* (OR-R) to compare the antibody-injected embryos to. Using DIC microscopy, I recorded video footage of lipid droplet transport in 15 embryos during phase II (see 4.1.1). Trajectories of 230 lipid droplets were tracked and the tracks were split into segments of uninterrupted motion in either direction or pauses using the methodology described in 4.5. In the following, I summarize the results I obtained by analyzing these tracks to obtain a quantitative description of normal transport that I will use as a reference for the antibody-injected embryos.

5.1.1 Run length distributions

The distance a droplet travels in one direction until it reverses motion or pauses is termed “run length”. This quantity is an important descriptor of bidirectional transport since the direction having the larger mean run length will be the direction of net transport. However, given that run lengths are not normally distributed (fig.5.1), determining the mean does not necessarily give a robust estimate because we only have a limited data set and small changes in the number of very long runs ($> 2 \mu m$) can have a significant influence on the result. Given a certain intrinsic run length distribution of the transport by motors, we might not be able to reproduce it even with a large amount of measurements. The reason for this is that the crowded environment in the cell will lead to obstacles for the motors on the microtubule, the droplet bumping into other cargos, or cargos travelling out of the field of view. All of these will decrease the amount of long runs, resulting in a high sensitivity of the mean to fluctuations in the number of long runs.

To avoid this shortcoming, previous work [16] has fitted the run length distributions for plus- and minus-end transport by the sum of two exponential decays (fig.5.1, fig.5.2). The advantage of this method is that it is robust against small changes at long run lengths as the fit parameters are mostly determined by runs shorter than about $1.5 \mu m$. An exponential distribution can be expected if there is a constant probability of a run to stop - due to detachment and/or attachment of an opposite motor. Gross et al. justified the choice of two exponentials with two different states of motion, a slow short-

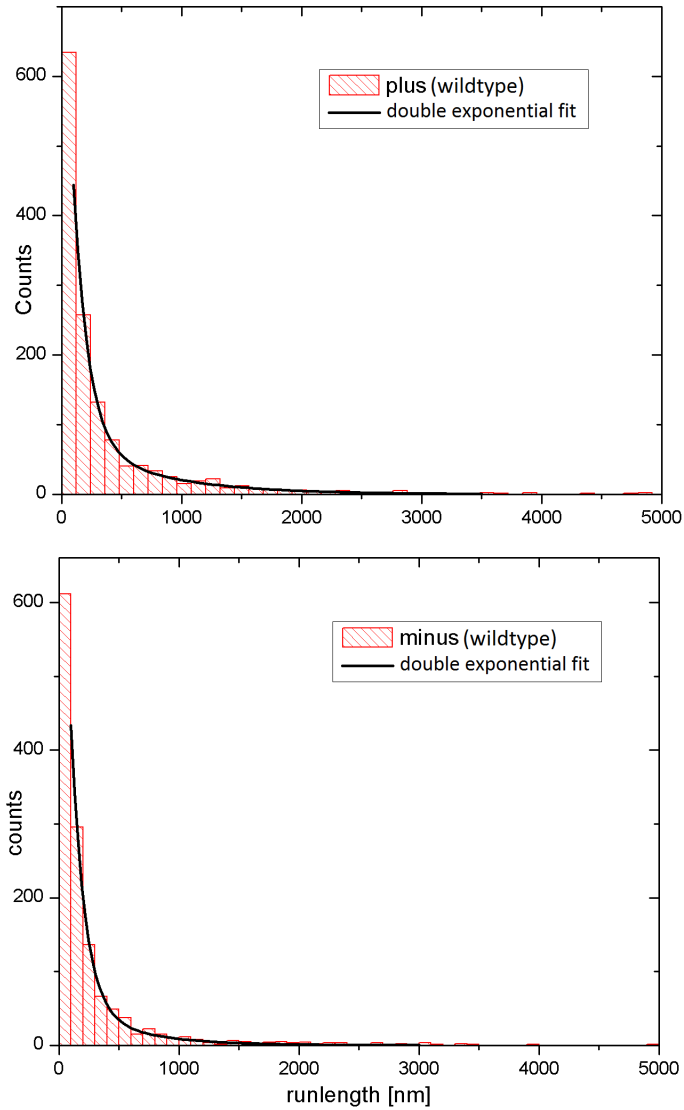


Figure 5.1: Plus- and minus-run length distributions of the reference data from wildtype *Drosophila* embryos. Each histogram was fit with a double exponential decay. The plus-end fit parameters were $D_{1+} = 701 \text{ nm}$ and $D_{2+} = 124 \text{ nm}$ with a reduced χ^2 value of 0.84 (top). Fitting the minus-runs (bottom) resulted in $D_{1-} = 495 \text{ nm}$ and $D_{2+} = 112 \text{ nm}$ at $\chi^2 = 1.75$.

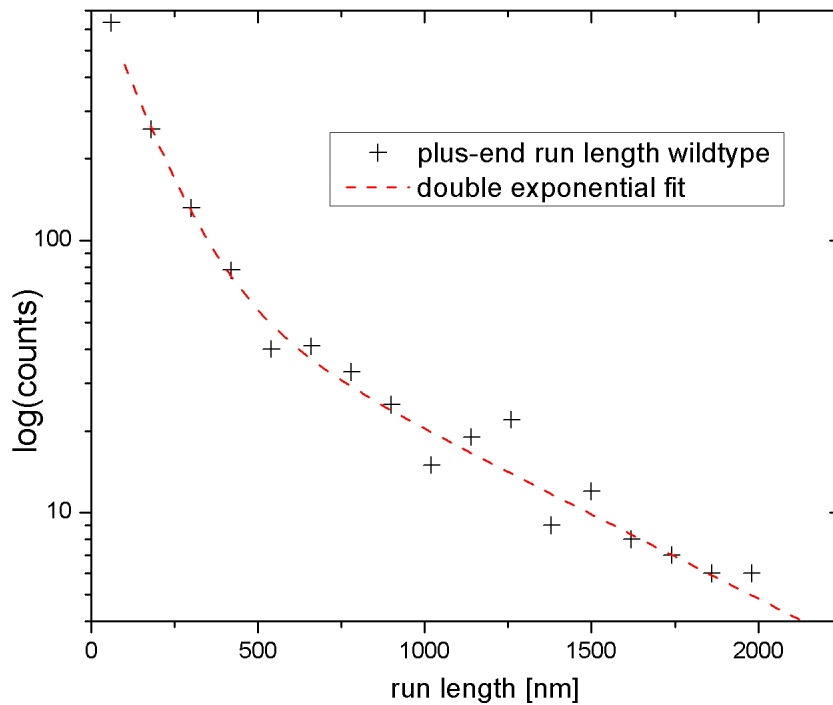


Figure 5.2: Plus-end run length distributions of the reference data from wild-type *Drosophila* embryos on logarithmic scale. It shows the same fit as in 5.1. As exponentials appear linear in this scaling, one can see that the data is well fit by the sum of two exponentials.

travel state (decay constant $< 100 \text{ nm}$) and a long-fast one ($\gg 100 \text{ nm}$). The long runs have been shown to be faster on average and the corresponding large decay constant determines the transport behavior as it changes significantly between different developmental phases [16] while the small decay constant remains essentially unchanged. Therefore both plus- and minus-end run length distributions were fit by

$$y(l) = A_1 \exp^{-\frac{l}{D_1}} + A_2 \exp^{-\frac{l}{D_2}} \quad (5.1)$$

with A_1 and A_2 being the amplitudes of the exponential decays with decay constants D_1 and D_2 . Only runs with velocities larger than $100 \frac{\text{nm}}{\text{s}}$ were included in the histograms. This is an arbitrary threshold, but everything faster than $100 \frac{\text{nm}}{\text{s}}$ is very likely due to active transport by motors. Moreover, if there are details missed or missinterpreted by our parsing program due to uncertainties in the tracking, they will mostly affect short segments. Therefore, we only use runs that are longer than 100 nm in the exponential fit. This gives us reasonable fits (quality is described by reduced χ^2 value) and characteristic run lengths (decay constants) which are presented in tab.5.1 together with values obtained previously using a similar method of data analysis [33]. Differences are likely due to the details of the analysis as described below.

The values in tab.5.1 are listed without uncertainties. This is because these values, while being good measures of the run lengths, are likely influenced by the way tracks are split into segments using Marathon (see 4.5.2).

Table 5.1: Runlengths in plus- and minus-direction for reference (OR-R), control (YW) and from [33]

dataset	plus-end transport			minus-end transport		
	D_1 [nm]	D_2 [nm]	χ^2	D_1 [nm]	D_2 [nm]	χ^2
OR-R	701	124	0.84	495	112	1.75
YW	728	92	0.93	524	112	0.85
Petrov[33]	852	78	0.86	503	62	1.76

The calibration of the program as well as the thresholds used for parsing and merging segments into runs can all influence the outcome. However, for a fixed set of parameters, the measured decay lengths are robust. This was demonstrated by analyzing two sets of data obtained from flies with no inherent difference in the transport machinery (YW, wildtype with different eye color). When analyzed the same way, the two sets gave run length values within a few percent of each other.

The robustness of run length as described above implies that it can be used to detect changes. This will be crucial to test my predictions for antibody-injected embryos. With no uncertainties, the significance of possible changes will be quantified using a randomisation t-test as described in 5.3.1.

5.1.2 Pause durations

Pauses are defined as “runs” with velocities $< 50 \frac{nm}{s}$ that last for at least $0.25 s$, which corresponds to ~ 7 frames of the video. Again, the as-

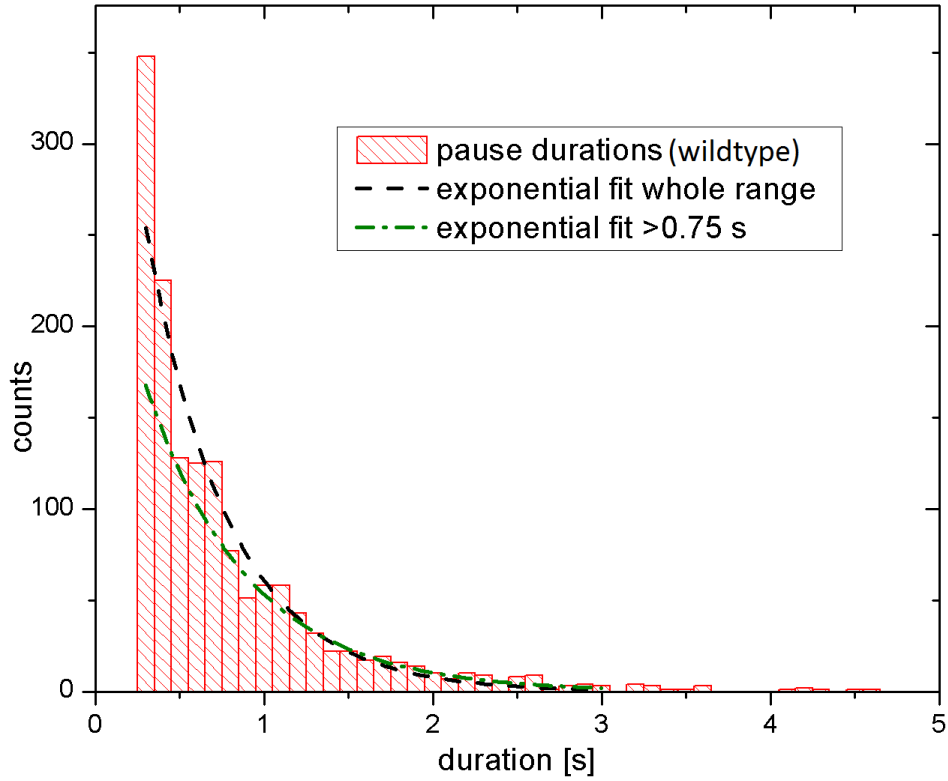


Figure 5.3: Pause durations for the reference data. The pause durations were fit by a single exponential decay. The fit resulted in a decay constant $\tau_{ALL} = 0.49$ s with $\chi^2 = 3.12$. Fitting only for pauses > 0.75 s improves the fitting quality to $\chi^2 = 1.04$ and gives $\tau_R = 0.61$ s. The bins start at 0.25 s because this is our threshold for pauses.

sumtion is that there exists a constant probability of the cargo to leave this state [16]. Therefore we fitted the pause duration distribution with a single exponential decay

$$y(t) = A_0 \exp^{-\frac{t}{\tau}} \quad (5.2)$$

with a characterisite pause duration τ . Fitting an exponential to the whole dataset gives us a pause duration of $\tau_{ALL} = 0.49 \text{ s}$ with a poor fitting quality of $\chi^2 = 3.12$. The distribution itself does not seem to follow a single exponential as proposed [16]. One reason might be the splitting of tracks into runs/pauses of at least 0.25 s , which might result in a higher weight in the first columns in the histogram. Therefore, I fit an exponential decay only to the higher pause durations ($> 0.75 \text{ s}$) - which are unlikely biased by data processing - and thus obtain (fig.5.3) a pause duration of

$$\tau_R = 0.61 \text{ s}$$

with a significantly improved fitting quality of $\chi^2 = 1.04$. This value is higher than that reported by Gross et al. for the same velocity threshold of $50 \frac{nm}{s}$ (namely $< 0.3 \text{ s}$) [16]. However, this difference is likely due to the different parsing method used and the fact that the authors only analysed pauses separating direction switching and excluded pauses during motion in one direction. The latter cannot be excluded in our case given that predictions

of the different models include a possible increase in pauses when one polarity motor is impaired.

5.1.3 Pause frequency

The frequency of pauses will be another criterion we can use to distinguish between the two models of transport. Therefore, I determine the relative amount of pauses compared to all runs as well as the number of pauses per unit time. Fig.5.4 shows the relative number of runs for different velocity ranges (i.e. the absolute number falling in a velocity range relative to the total number of runs). I distinguished between runs in the plus- and minus-directions, and pauses. For the sake of completeness I also included the regime in between, but those segments are not used for the analysis as explained in the figure caption. As one can see, 30.5% of all runs are pauses. The relative distribution for the different velocity ranges will enable us to distinguish between changes in pause characteristics caused by an overall change in this distribution and changes independent of it (e.g. if pauses are increased at the expense of plus-end runs). In addition to the relative number of pauses, the number of pauses per unit time, is also quantified:

$$f_R = \frac{N_{pause}}{T} = \frac{1477}{4085.06 \text{ s}} = (0.362 \pm 0.018) \text{ s}^{-1}$$

The total time measured has a negligible error compared to the absolute number of pauses. The uncertainty of the latter depends on the parsing process of the tracks and is hard to estimate. However, the pause frequency be-

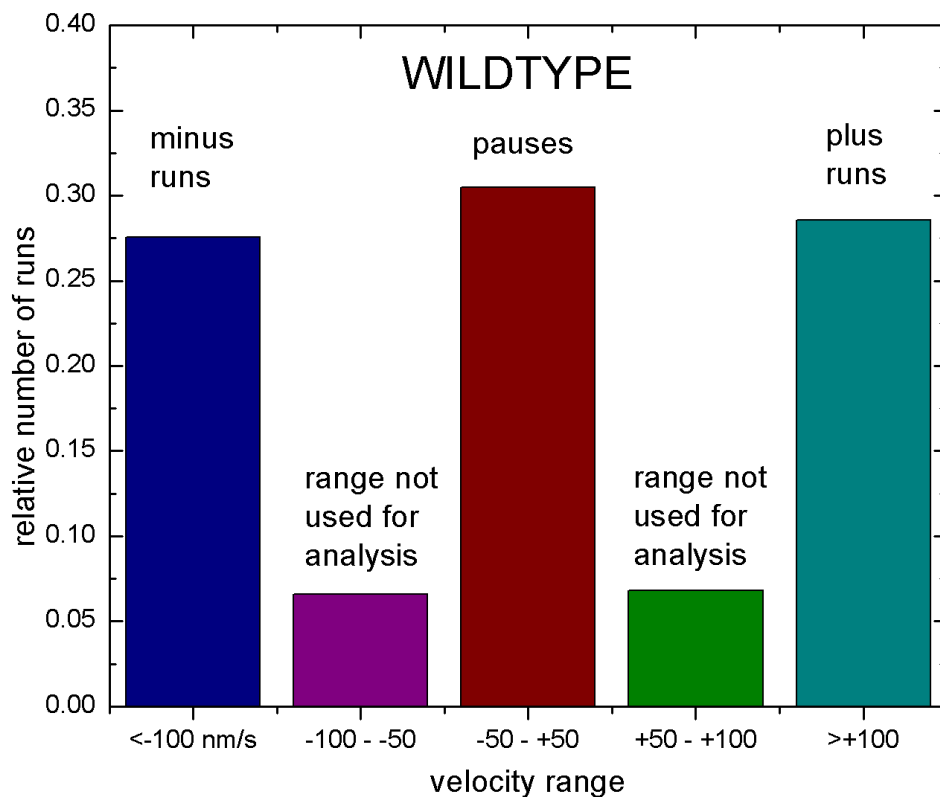


Figure 5.4: The relative number of runs as a percentage of the total number of runs ($n = 4842$) are split for the different velocity ranges shown. 30.5% of the runs are pauses and the ratio between plus- and minus-end runs is $\frac{N_+}{N_-} = 1.04$. Runs with velocities between $50\frac{nm}{s}$ and $100\frac{nm}{s}$ are not used for the analysis of run lengths, given that they can be due to artifacts other than motor-driven transport. Their relatively small number and equal distribution between the opposite directions justifies their omission.

tween different tracks does vary as well as the duration of the different tracks. Therefore, I determined the error with a bootstrapping method: Having N tracks, I randomly chose N tracks with repetition from the pool of all tracks and determined their pause frequency. Continuous repetition of this results in a gaussian distribution with a standard deviation determining my error. Furthermore, I characterize the ratio of plus- and minus-end runs (faster than $> 100 \frac{nm}{s}$) to be

$$\frac{N_+}{N_-} = 1.04$$

Even though the number of runs in each direction is almost equal, the net transport during this phase of development is towards the plus-direction because of the larger plus-end run length as determined above (fig.5.1).

5.1.4 Velocity distributions

The histograms in fig.5.5 show the velocity distributions for plus- and minus-end transport during phase II of embryo development. Given the lack of a complete understanding of transport mechanisms, there is no general agreement on which mathematical model describes these distributions. Some report peaks in velocity histograms caused by integer numbers of motors (~ 10) [23][25]), working against opposing load, but these distributions are not typical and can be a result of poor analysis [28]. No significant peaks are visible in fig.5.5. To characterize velocities consistent with previous reports [51], I will

use the mean velocity of the runs weighted by their duration. These values have been published before [51], so I can compare my analysis to previous experiments. The weighting was calculated as follows:

$$\begin{aligned}
 \bar{v}_+ &= \sum_{v_i > v_T} v_i \cdot w_i \\
 \bar{v}_- &= \sum_{|v_i| > v_T} v_i \cdot w_i \\
 \Delta v &= \sqrt{\frac{1}{N^2} \sum_i (v_i \cdot w_i - \bar{v})^2}
 \end{aligned} \tag{5.3}$$

where $w_i = \frac{t_i}{\sum_i t_i}$ are the weights. Uncertainties Δv are weighted standard errors of the mean. The weighted velocity is insensitive to the factors detailed in 5.1.1 that render mean run length a poor descriptor of transport. For the weighted velocity I again only consider runs faster than $100 \frac{nm}{s}$. The values are reported in tab.5.2 . I also included weighted velocity values of all runs faster than $50 \frac{nm}{s}$ to be able to compare to previous work on the same system. The mean weighted velocities of my reference data are, within errors, in agreement with the previously published values [51]. The values for the $100 \frac{nm}{s}$ threshold are higher, as can be expected if you leave out the ambiguous uncertain range $50 - 100 \frac{nm}{s}$ (see fig.5.4).

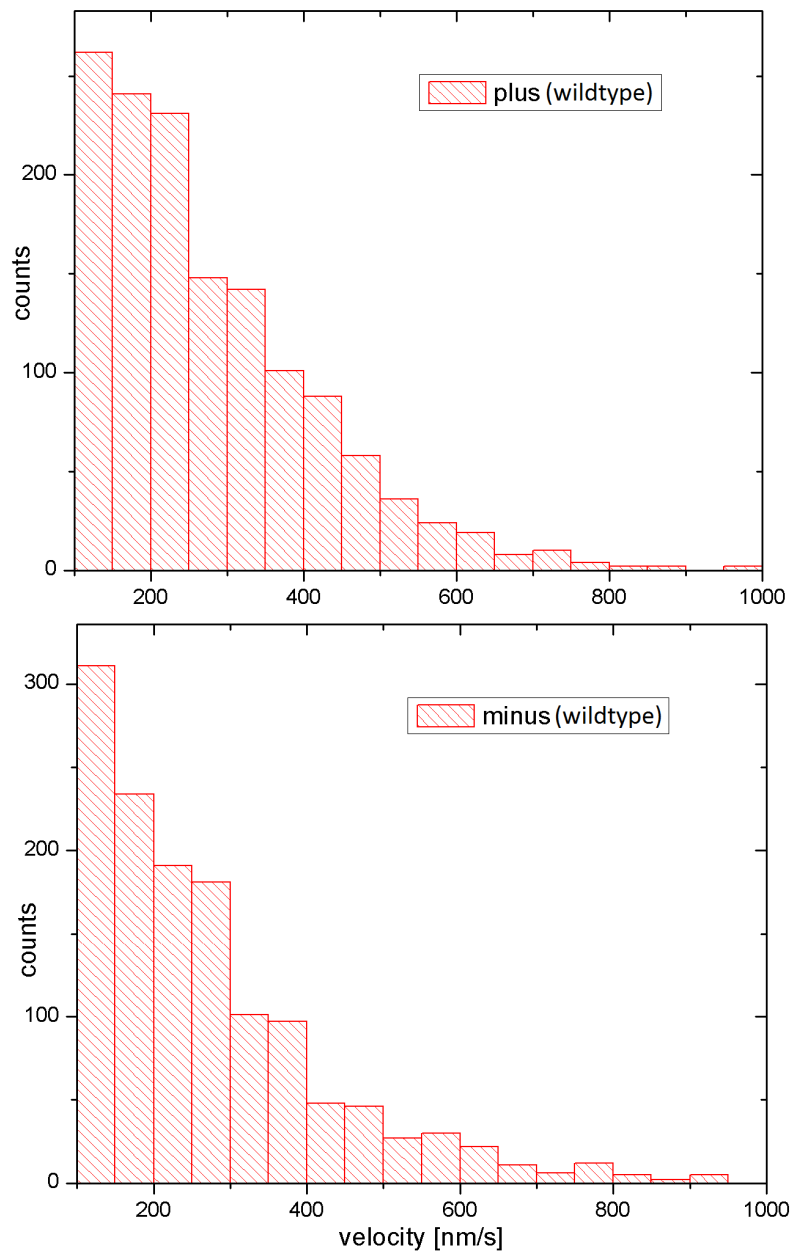


Figure 5.5: Histograms of the velocity distribution of runs ($> 100 \frac{nm}{s}$) for plus- and minus-end transport during Phase II. The mean velocities weighted by their duration are $\bar{v}_+ = 341 \pm 9 \frac{nm}{s}$ and $\bar{v}_- = 349 \pm 10 \frac{nm}{s}$.

Table 5.2: Weighted mean velocities of droplet transport for reference measurements of Phase II embryos

threshold	100 $\frac{nm}{s}$	50 $\frac{nm}{s}$	
	\bar{v}_R [$\frac{nm}{s}$]	\bar{v}_R [$\frac{nm}{s}$]	Welte[51] [$\frac{nm}{s}$]
plus	341±9	317±8	321±15
minus	349±10	315±8	359±50

5.2 Effect of injection of anti-*Kinesin* antibodies

5.2.1 Injection of antibodies - large scale

The image sequence in fig.5.6 shows the temporal evolution of an embryo injected with antibodies against *Kinesin*. It can be clearly seen that the injection area (right side of the embryo) develops differently and the transport of droplets to the periphery (dark clouded periphery) only takes place on the side of injection. This sample was imaged for a longer time than what is usable for particle tracking. Given that the embryo is still developing, it grows past phase II in about 15 minutes post-injection. However, the effect was not always this uniform. Usually, only smaller parts of the periphery close to the injection point reclouded (fig.5.7) which is probably due to variations in the injection volume, the antibody concentration and the injection efficiency. As I mentioned above (see 4.3), the embryo is squashed between the glass slide and a coverslip. Due to the injection process, the membrane of the embryo is already damaged and, therefore, some of the cytoplasm leaks out, which is likely to contain part of the antibodies. For these reasons, high magnification videos

only from areas that definitively showed reclouding were taken into account for single particle tracking and analysis.

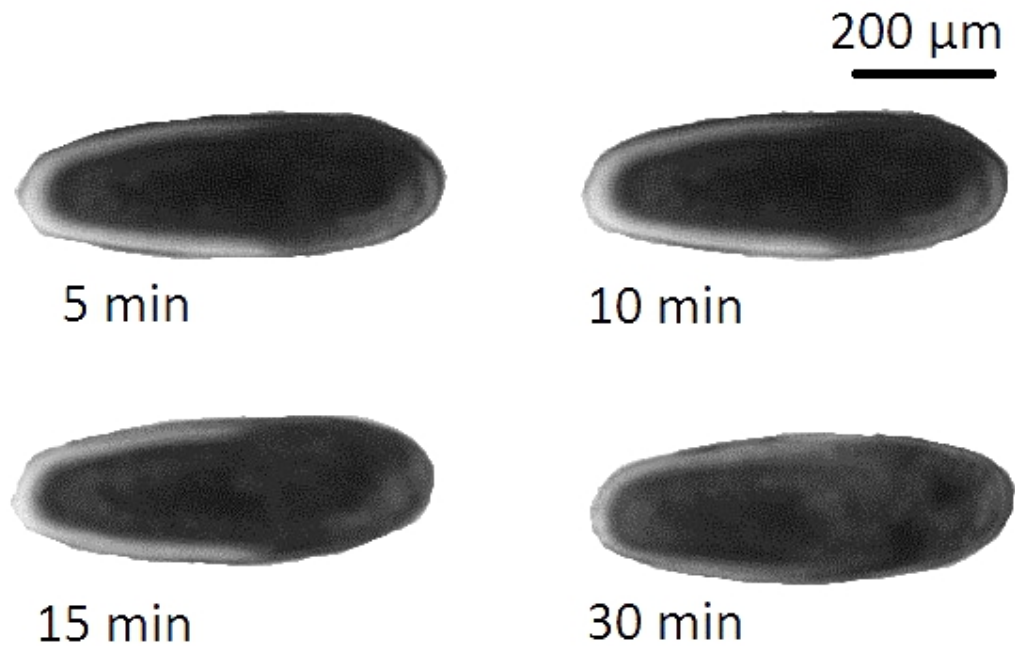


Figure 5.6: Development of an Embryo injected with antibodies against kinesin. In the area of injection (right side) lipid droplets have been transported to the outside of the embryo making it appear cloudy (dark) while the periphery on the opposite side still remains clear. Indicated times are times post-injection.

5.2.2 Injection of antibodies - single droplet scale

Using high magnification DIC microscopy, it was possible to detect the injected areas of an embryo just by looking at the lipid droplets distribution in the periphery. Unlike the distant unaffected areas or untreated embryos



Figure 5.7: Image of an embryo injected with antibodies against *Kinesin* after recording the high magnification images. The reclouding is only local and less strong than for the example in fig.5.6. The reason for this is most likely leaking out of antibody solution due to squashing the embryo between the coverslip and glass slide for imaging. For many embryos, the reclouded area was even smaller.

(fig.4.9), the periphery was already crowded with droplets during a developmental phase where it usually is clear. Nevertheless, after recording the high magnification videos, the effect of the antibody was double checked by looking at the embryo as a whole, and only videos that showed a crowded periphery both on large scale and single droplet scale were analyzed. The fact that it was already crowded by the time I started imaging, was due to the time it took me to prepare the sample, post injection, for DIC microscopy ($\sim 2min$). As one can see from the tracks in fig.5.8, most of the droplets still show bidirectional motion. This most likely means, that not all *Kinesin* was blocked with an antibody. However, the overall transport has clearly changed. Hence, even if *Kinesin* is only partially inhibited, I should still be able to detect changes in the transport characteristics.

The crowded field of view has both advantages and disadvantages over the sparse, uninjected images for the reference embryos: On the one hand

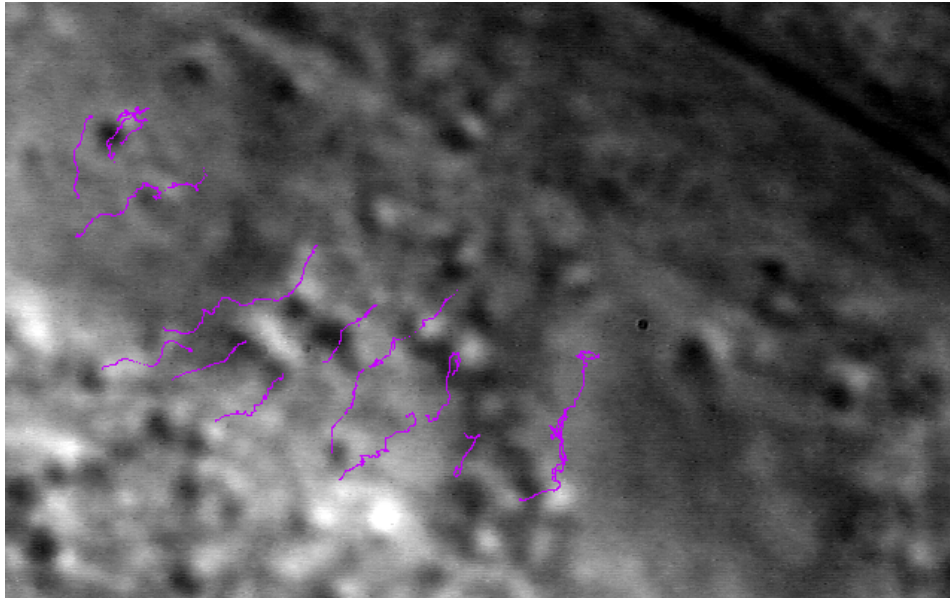


Figure 5.8: Picture from a Phase II video of lipid droplet transport in the periphery of a *Drosophila* embryo injected with anti-*Kinesin* antibodies. Unlike embryos that were not injected with antibodies (fig.4.9), the field of view is already crowded with lipid droplets, implying biased transport towards the minus-end (top right). The purple lines represent the tracks obtained from this video. The residual transport in the plus-end direction (bottom left) indicates that not all *Kinesin* molecules were blocked. Nevertheless, global transport is obviously favoring *Dynein*.

one has a large number of droplets for tracking. But on the other hand, tracking them is a lot harder as the density of droplets leads to more bumps between droplets and more motion of droplets in- and out-of-focus. In addition, sometimes the videos were blurred by the leaked cytoplasm that was creating a layer over the injected area. Therefore, tracks from these videos can be expected to be - on average - shorter than for the reference. But as we discard the first and last run of each track for analysis anyway, this should not bias

our results given that most tracks are comprised of many runs and pauses. Moreover, the suppression of very long runs has no influence given the way we determine the characteristic run length (see 5.1.1).

5.3 Transport characteristics of embryos injected with antibodies

5.3.1 Run lengths

The tracks obtained from the videos of injected embryos are analyzed in the same way as the reference data. Again, a double exponential decay is fitted to the run length distribution for motion towards the plus- and the minus-end. The histograms with fits are shown in fig.5.9 and the fit parameters are listed in tab.5.3 together with those of the reference data.

Table 5.3: Runlengths in plus- and minus-direction for samples injected with antibodies and comparison to the reference data

		reference [nm]	injections [nm]	χ^2	p-value
plus	D_1	701	312	0.77	0.008
	D_2	124	57		
minus	D_1	495	608	0.86	0.034
	D_2	112	82		

Due to the antibodies against the kinesin heavy chain the plus-end run length is decreased. *Dynein*-driven motion, on the other hand, is increased compared to reference data. The longer run length for minus- compared to plus-end transport in the injected embryos is expected given the crowded pe-

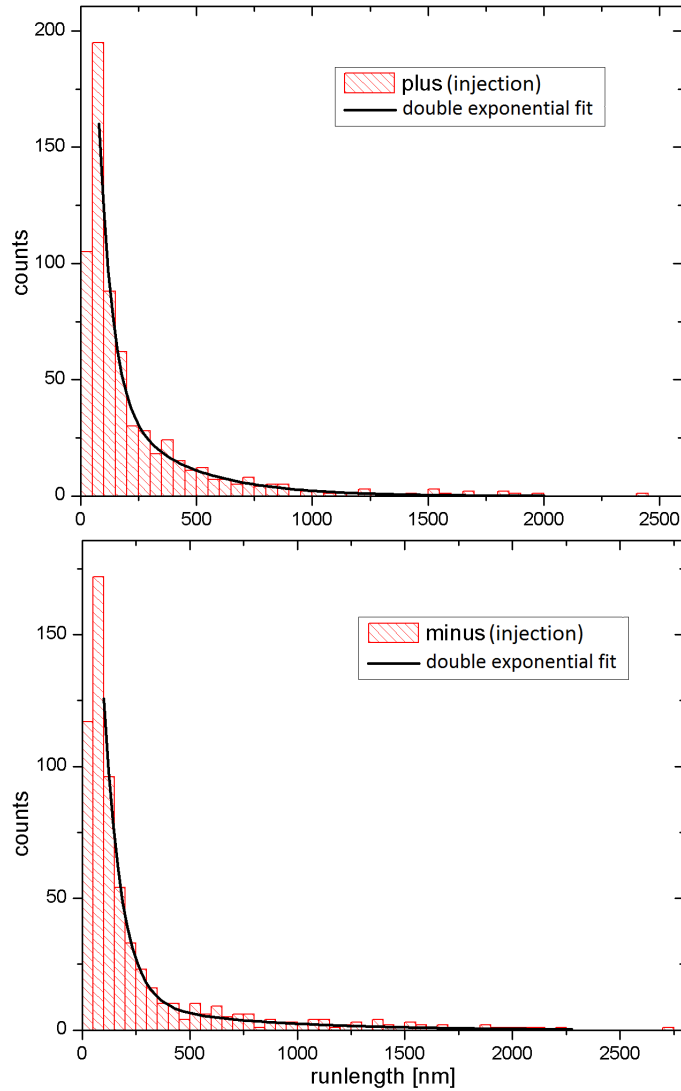


Figure 5.9: Plus- and minus-end run length distributions of lipid droplets after injection. Double exponential fits resulted in decay lengths of $D_{1+} = 312 \text{ nm}$ and $D_{2+} = 57 \text{ nm}$ with a χ^2 value of 0.77 for plus-end runs (top). The results for minus-runs (bottom) are $D_{1-} = 608 \text{ nm}$ and $D_{2-} = 82 \text{ nm}$ at $\chi^2 = 0.86$.

riphery we see after injections. The dominance of plus-end (=inward) transport is undermined by antibodies. To check if these changes, independently from the exponential fit, are significant, I use a *randomisation t-test*: the two data sets of run lengths are merged to one pool of data and then randomly two groups of the size of the initial data sets are drawn from that pool. The difference in their mean is determined and the whole process is repeated several thousand times. This results in a normal distribution of differences in the mean values which is compared to the difference between the mean values of our initial data sets. Depending on the relative position to the distribution a p-value is assigned, which indicates the probability that both data sets originated from the same distribution. Unlike in a normal *t-test*, the datasets do not need to be normally distributed [8]

As I mentioned earlier, the mean is sensitive to fluctuations in long run lengths, hence we do not include long runs for the significance test. We just use a window in the distribution which is unlikely to be biased by the data processing (i.e. short runs, and tail values in the distribution, where the count is small). Therefore, I chose the range 250 – 1250 *nm* to compare plus-end runs and 250 – 1500 *nm* for minus-end runs, resulting in $p = 0.008$ and $p = 0.034$ respectively. This means that both changes - decrease of plus-end motion and increase of minus-end motion - are statistically significant. In order to validate this test, I compared the distributions for plus- and minus-end after injection ($p = 0.034$), which is expected given that the distributions are unique. Moreover, to check the ability of the test to detect similar distri-

butions, I randomly split each distribution in half and ran the test on both halves. Comparison of the resulting datasets for plus-motion gave $p = 0.977$, the ones for minus-motion $p = 0.93$ - thus proving that data from the same distribution can actually be detected using the randomization t-test..

5.3.2 Pause durations

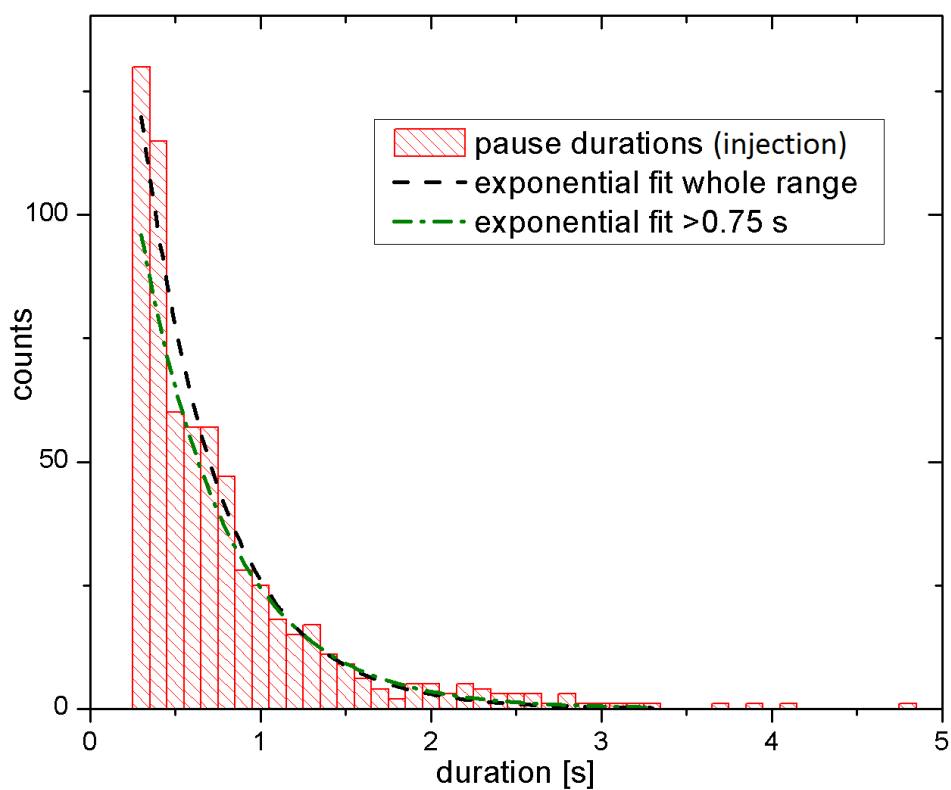


Figure 5.10: The pause durations of the lipid droplet tracks after injection of the antibody were fit again to a single exponential decay. A pause duration of $\tau_{ALL} = 0.46 s$ with $\chi^2 = 1.07$ was obtained for the whole range and $\tau_I = 0.46 s$ with $\chi^2 = 0.82$ for fitting pauses longer than 0.75 s.

We determine the pause duration for the tracks after antibody injection as described for reference data in 5.1.2. An exponential fit to pauses with $v < 50 \frac{nm}{s}$ and a minimum duration of $0.25 s$ results in $\tau_{ALL} = 0.46 s$ at $\chi^2 = 1.07$. Even though this χ^2 value implies a good fit, we can see the same shoulder structure in the histogram observed for the reference data at about $0.7 s$ (fig.5.3). Therefore, we fit with an exponential decay only for pause durations $> 0.75 s$ (fig.5.10). This results in

$$\tau_I = 0.51 s$$

with a reasonable fit quality of ($\chi^2 = 0.82$). This pause duration is smaller than the value of $\tau_R = 0.61 s$ I determined for my reference data. Just like in the paragraph above we use the randomization t-test to find the probability that both datasets originate from the same distribution. With $p = 0.263$ for the range I used for the fitting, this change is not statistically different, even though one can see a trend to lower pause durations.

5.3.3 Pause frequency

Similar to uninjected embryos, I determined the relative number of pauses and runs lying in the different velocity ranges. When compared to fig.5.4, fig.5.11 shows that there is no major change due to the antibody injection for the relation between pauses and runs. Pauses comprise almost a third of the events and the plus- and minus-runs are observed with equal proportions. This also means that the decreased pause duration is not caused by

a shift of runs with a short duration into the pause region, but rather by a change of the nature of pauses.

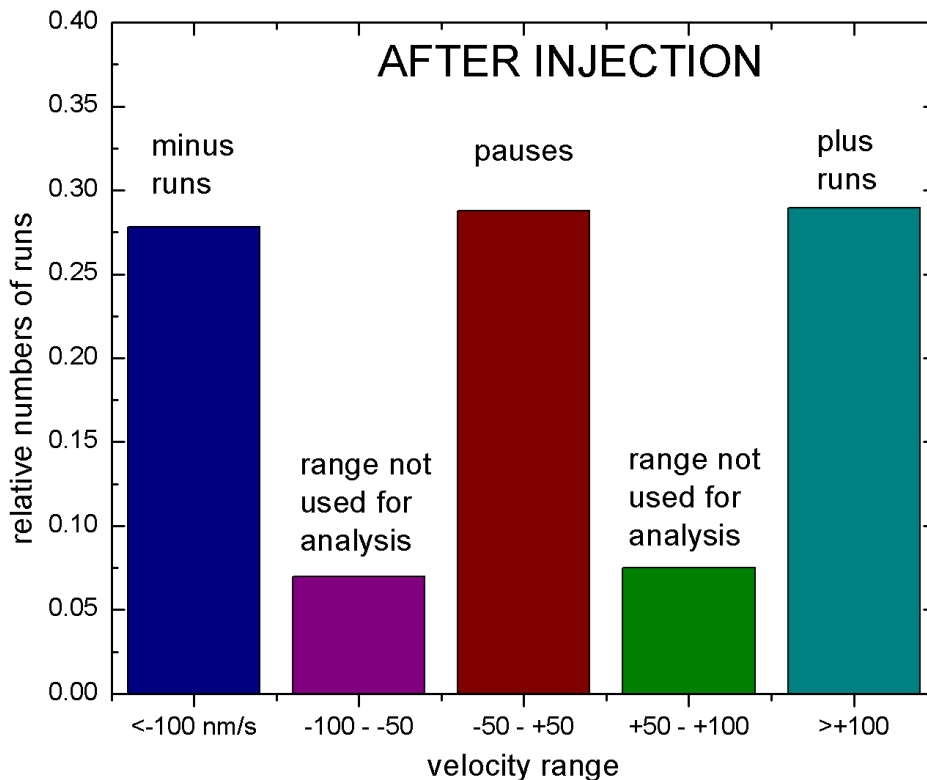


Figure 5.11: Relative number of runs in different velocity ranges compared to the total number of runs ($n = 2253$) after injection of antibodies. 28.8% of the runs are pauses and the ratio between plus- and minus-runs is $\frac{N_+}{N_-} = 1.04$. There are no obvious changes in this graph compared to the one obtained from reference data (see fig.5.4)

The pause frequency

$$f_I = \frac{648}{1675.81 \text{ s}} = (0.387 \pm 0.025) \text{ s}^{-1}$$

is slightly higher than the one for the reference data, but still within the errors. The next values I probe for changes are the ratio between *Kinesin* and *Dynein* mediated runs

$$\frac{N_+}{N_-} = 1.04$$

The number of plus-end runs to minus-end runs remains constant compared to the reference data.

5.3.4 Velocity distributions

The histograms for the velocity distributions after the injection of antibodies are shown in fig.5.12. Compared to the wildtype data (fig.5.5), the distribution appears to remain qualitatively similar. To quantify possible changes, I calculated the mean weighted velocities for this dataset like described in section 5.1.4. The results are presented in tab.5.4.

Table 5.4: Weighted mean velocities of droplet transport for Phase II embryos after injection (velocity threshold $100 \frac{nm}{s}$). \bar{v}_R and \bar{v}_I are the weighted mean velocities for reference data and data after injections respectively

	\bar{v}_R	$\bar{v}_I [\frac{nm}{s}]$	change
plus	341 ± 9	289 ± 12	-15.0%
minus	349 ± 10	325 ± 13	-7.9%

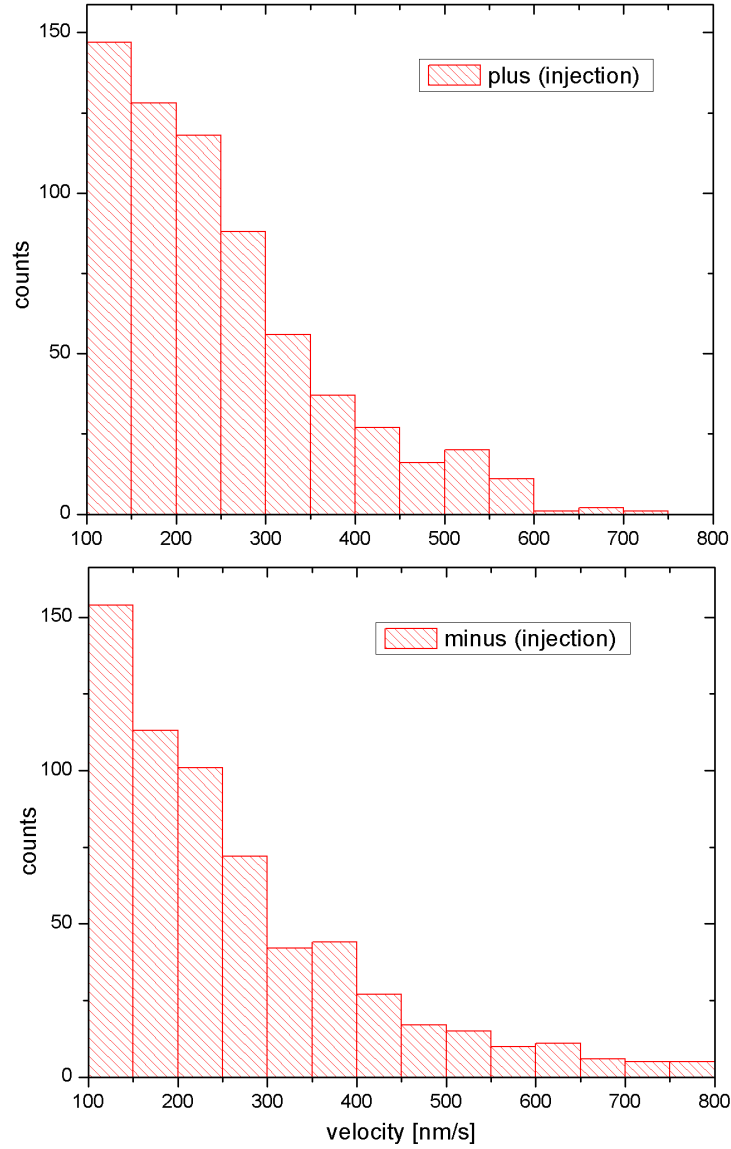


Figure 5.12: Histograms of velocities of runs ($> 100 \frac{nm}{s}$) for plus- and minus-end transport during Phase II after injection of antibodies.

The velocities in both directions are slightly reduced, more for *Kinesin* (−15%) than for *Dynein* (−8%).

5.4 Discussion

At this point I first want to summarize the effect of antibody injection on transport characteristics, followed by a possible interpretation. The analysis in the sections above showed the following results:

- the minus-end run length is significantly increased (+23%)
- the plus-end run length has significantly decreased (−55%)
- pause durations after injection show the tendency to be shorter
- the frequency of pauses is barely increased
- the relative amount of pauses compared to all runs has slightly decreased
- the ratio between the number of runs in plus- and minus-direction remains constant
- the velocity of runs is reduced, more for plus- than for minus-end (−15%/−8%)

First, I will compare these results to observations reported in previous publications. In similar experiments, but different system the same antibodies have been reported to inhibit both plus- and minus-end directed transport [42]. But in their system (chicken dorsal root ganglia), *Kinesin* is responsible

for the vast majority of transport, which could be the reason, that they barely saw *Dynein*-mediated motion after injections. In my system on the contrary, transport by *Dynein* is increased.

A similar, but more drastic decrease in velocities has been reported by Brady et al [6] for transport of membrane bounded organelles in squid axoplasm, where they perfused their sample with an *IgG* antibody against the heavy chain of squid kinesin. This resulted in a decreased velocity over time for both plus-(-54%) and minus-end (-28%) transport after 30-60 minutes, but also in an already significant velocity drop after 10 minutes ($\sim -25\%$), which is more comparable to my timescale, but still more velocity decrease than I detect. The main points I am interested in, run lengths and pause durations, were not measured in their experiment. However, another study using antibodies against *Dynein* in order to check for attachment to microtubules of purified vesicles *in vitro* did not report any velocity changes [18].

In the following, I discuss how these results fit to the predictions I made for the two models of transport (see 3.3). Overall it has to be noted that the bidirectional motion of most cargos indicates that only some of the *Kinesins* have been impaired by antibodies. However, the changes in several transport characteristics after the injection demonstrate the effect of the antibodies. For several of the observed values the predictions of both models diverged.

5.4.1 Comparison to *regulation*

For a *regulation* model we would have not expected that the minus-end run length is increased because transport in each direction would be regulated and thus, disabling *Kinesin* would not alter minus-end transport at all. The decreased plus-end run length would only agree with a *regulation* model if the run length depends on the number of *Kinesins* present on a cargo (less motors=shorter distance). This is the case *in vitro* [47], but has been reported not to be the case in my system *in vivo* [38]. However, given that the latter work used genetic reduction of *Kinesin* dosages rather than disabling existing ones as we do in this work, indirect interference cannot be excluded.

Pauses tend to be shorter, even if the change is not statistically significant. This is contrary to the *regulation* model, which predicted an increase due to additional pauses substituting plus-runs. But considering that apparently only a fraction of *Kinesin* is blocked, no change in the pause durations and in the ratio between the numbers of plus- and minus-runs are in accordance with this model. The fact that pause frequencies are not altered also matches the *regulation* model.

The reduction in velocity of runs in both directions, even though more significant for *Kinesin* than *Dynein*, also favors *regulation* as the *Kinesin*-specific antibody does not attach to *Dynein*. Therefore, the reduced velocity of the minus-end motor has to be caused indirectly - either by regulation process trying to adapt *Dynein*'s velocity to *Kinesin*'s or by a higher drag force on the cargo. The latter could be caused by an increased viscosity due

to adding the antibody solution, which would result in an increased drag and a subsequent slowing down of the motors.

Therefore, in order for *regulation* to be in accordance with my data, some requirements need to be fulfilled: there needs to be some mechanism that can explain the increase of the *Dynein* run length. This could possibly be a switch whose concentration can change the run characteristics and the injection alters this concentration. The reduced *Dynein* velocity might be caused by regulation, but the decrease in *Kinesin* velocity and run length would need either a viscosity increase or possible interference of the antibody. Moreover, it would be necessary that the regulation mechanism senses if a motor cannot walk in order to maintain the pause durations, which show no sign of increase.

5.4.2 Comparison to *tug-of-war*

Predictions from a *tug-of-war* model on the other hand match with an increased run length for minus-end transport as there are less *Kinesins* able to attach to the microtubule and fight *Dynein*. For the decrease in plus-run length we run into the same problem described in 5.4.1. Just because we expect less plus-runs does not mean the ones that exist have to be shorter. One possible explanation would be that the antibody simply decreases the ATPase activity and does not keep *Kinesin* from attaching to the microtubule in the first place. This would explain the lower *Kinesin* velocity and run length, but our *in vitro* experiments indicate that the antibodies prevent microtubule

attachment, matching with previous publications [42]. However, the way the antibody works needs to be analyzed in more detail *in vitro*.

The trend in the pause duration can also be explained with this model: *tug-of-war* situations, which make up part of the pauses, are expected to be resolved faster in favor of *Dynein* winning, because there are on average less *Kinesins*. For cases where *Kinesin* wins, they will last the same amount of time as we do not alter the numbers of *Dynein* motors. Due to the only partial inhibition of *Kinesin*, this is likely to be only a minor change. If most plus-end motors were disabled, a decrease of pause frequencies would have been expected, caused by longer minus-runs and only a few plus-runs. But as there is no significant reduction in the number of plus-runs in my experiments, no real prediction can be made and this neither supports nor contradicts this model.

However, there are observations which are not easily compatible with a *tug-of-war*. If there are on average less *Kinesins* participating in a *tug-of-war*, it would be expected that the relative number of plus-runs compared to minus-runs decreases because *Dynein* wins more often. I do not see a change in this ratio after injection. This might also be explained by only some of the *Kinesin* being disabled: In the majority of *tug-of-wars*, the outcome is the same as without injections. Only situations, where *Dynein*'s position against *Kinesins* is strongly improved (e.g. in numbers), are resolved very fast. If these situations only make up a smaller fraction of the pauses it might not be reflected strongly in the comparison between plus- and minus-run numbers

and would also be in accordance with the only insignificant decrease of pause durations. Although this explanation seems to contradict an effect on the run length, it is still compatible: the increase in minus-end runs is small, but significant, and is still far away from the *in vitro* value for multiple *Dynein* motors (several μm) [21]. The decrease in the *Dynein* velocity is incompatible with this model as there should be no crosstalk between *Kinesin* and *Dynein*. However, proposing a higher drag force due to an increased viscosity resulting from the injection might resolve this problem.

In order for this model to match my results, the drag force on the lipid droplets would need to be increased. This would account for the slight velocity decrease in both directions and thus also could explain the shorter run length of *Kinesin* (higher detachment rates). This could be caused by a higher viscosity due to the antibody injection or by transport of other cargos - not visible in DIC - towards the minus-end, increasing the density of obstacles for the droplets.

Summing up, neither a plain regulation nor a tug-of-war model alone can fully explain all of my observations. However, especially because of the significant increase of the minus-end run length and less additional requirements, my data is favoring a *tug-of-war* model.

Chapter 6

Conclusion and future work

6.1 Summary and conclusion

In this thesis I probed the coordination mechanism of the two microtubule based molecular motors. Each of them can only walk towards one specific end of microtubules (*Kinesin* moves towards the plus-end, *Dynein* towards the minus-end). My goal was to test the two models that exist to date to explain bidirectional intracellular transport. My approach consists of introducing a concentrated solution of function-blocking antibodies against *Kinesin* in living cells and comparing the observed changes in transport characteristics to the predictions of the two models.

The first model, *Regulation*, is based on a regulatory complex that controls the motion, while the *tug-of-war* model only relies on the molecular motors and their properties. The main difference between the models is that, for *regulation*, the change in direction is controlled, meaning only one motor type at a time is “on”. In the *tug-of-war* model the opposite polarity motors stochastically engage in fights, in which only their properties, like force and detachment rate - which can differ during development - determine the transport behavior. The most significant difference in predictions of the two models

for a situation where one motor is disabled are regarding the run length of the remaining motor (in my case *Dynein*) and the duration of pauses. *Regulation* does not predict changes in the minus-end run length unlike the *tug-of-war* model which expects an increase. For *Regulation*, pauses are supposed to last longer while for a *tug-of-war* scenario no change or maybe shorter pauses are expected.

In order to test these models, I injected anti-*Kinesin* antibodies into *Drosophila* embryos and recorded videos of motion of lipid droplets transported bidirectionally by these motors. The videos were analyzed using a tracking program for the lipid droplets and the obtained tracks were subsequently split into pauses, runs towards the plus- and the minus-ends of microtubules. From these runs I could determine characteristic features of the transport and compare them to the transport of droplets in embryos that were not injected.

Analysis of the data revealed that only a fraction of *Kinesin* was disabled by the antibodies as residual plus-end motion persisted. Nevertheless, significant changes in the transport characteristics could be detected. The comparison between my reference data and data obtained after injections showed the following results: while plus-end transport was strongly reduced, the minus-end run length was significantly increased. Pause durations showed an insignificant trend towards shorter pauses. Moreover, the pause frequency and the ratio between plus- and minus-runs remained the same and velocities of the motors in both directions were slightly reduced.

In the end, neither the *Regulation* nor the *tug-of-war* model alone is

able to explain all my results. Overall, observed changes match the predictions of the *tug-of-war* model better than the ones for *regulation*. Measurements incompatible with a *tug-of-war* can be explained by indirect effects due to the injection.

6.2 Outlook

While the conclusions of this work tend to favor the *tug-of-war* model, a few control experiments are still needed. The actual effect of the antibody needs to be characterized - even though our *in vitro* experiments indicated that it inhibits microtubule-attachment, a different way of interacting with *Kinesin* might change the interpretation. In addition, these results should be compared to the effect of anti-*Dynein* antibodies on the same system. Furthermore, an important control experiment will be the analysis of transport after injection of a control antibody at similar concentration that neither targets *Kinesin* nor *Dynein*. Even though this is reported not to alter transport on the large scale [38], it could support my conclusion by reducing motor velocities - or contradict it by influencing the run lengths. Moreover, experiments with higher concentrations of motor-targeting antibodies could also be used to test if the observed effect can be increased.

In the bigger picture, there are still many open questions for the transport by molecular motors. The interaction between opposite polarity motors is still not fully understood. Determining their coordination to achieve bidirectional motion is only a first step. It is, for example, still unclear how cells

manage to achieve different distributions for different cargos in the cytoplasm, while they are all carried by the same transport system. New mutations continue to be reported where certain genes have an influence on the transport characteristics, whether it be directly or indirectly. Thus, more work will be needed to reveal the intricacies of this amazingly robust yet versatile process in living cells.

Bibliography

- [1] Nascimento AA, Roland JT, and Gelfand VI. Pigment cells: a model for the study of organelle transport. *Annu Rev Cell Dev Biol*, 19:469–91, 2003.
- [2] Shabeen Ally, Adam G. Larson, Kari Barlan, Sarah E. Rice, and Vladimir I. Gelfand. Opposite-polarity motors activate one another to trigger cargo transport in live cells. *J. of Cell Biology*, 187:1071–82, 2009.
- [3] Charles L. Asbury, Adrian N. Fehr, and Steven M. Block. Kinesin moves by an asymmetric hand-over-hand mechanism. *Science*, 302:2130–34, 2003.
- [4] George I. Bell. Models for the specific adhesion of cells to cells. *Science*, 200:618–27, 1978.
- [5] Steven M. Block, Lawrence S. B. Goldstein, and Bruce J. Schnapp. Bead movement by single kinesin molecules studied with optical tweezers. *Nature*, 348:348–52, 1990.
- [6] Scott T. Brady, K. Kevin Pfister, and George S. Bloom. A monoclonal antibody against kinesin inhibits both anterograde, retrograde fast axonal transport in squid axoplasm. *PNAS*, 87:1061–65, 1990.

- [7] Simon L. Bullock, Daniel Zicha, and David Ish-Horowicz. The drosophila hairy rna localization signal modulates the kinetics of cytoplasmic mrna transport. *The EMBO Journal*, 22:248494, 2003.
- [8] G. Cardillo. Rndttest: An alternative to student t-test assessing difference in means. <http://www.mathworks.com/matlabcentral/fileexchange/20928>, 2008.
- [9] Brian C Carter, George T Shubeita, and Steven P Gross. Tracking single particles: a user-friendly quantitative evaluation. *Physical Biology*, 2:60–72, 2005.
- [10] Gabriel T. Dagani, Kate Monzo, Jean R. Fakhoury, Chung-Chu Chen, John C. Sisson, and Xiaojing Zhang. Microfluidic self-assembly of live drosophila embryos for versatile high-throughput analysis of embryonic morphogenesis. *Biomed Microdevices*, 9:681–94, 2007.
- [11] Sean W. Deacon, Anna S. Serpinskaya, Patricia S. Vaughan, Monica Lopez Fanarraga, Isabelle Vernos, Kevin T. Vaughan, and Vladimir I. Gelfand. Dynactin is required for bidirectional organelle transport. *Journal of Cell Biology*, 160:297–301, 2003.
- [12] Adams MD et al. The genome sequence of drosophila melanogaster. *Science*, 287:2185–95, 2008.
- [13] Susan P. Gilbert, Martin R. Webb, Martin Brune, and Kenneth A. Johnson. Pathway of processive atp hydrolysis by kinesin. *Nature*, 373:671–

76, 1995.

- [14] S P Gross, M A Welte, S M Block, and E F Wieschaus. Coordination of opposite-polarity microtubule motors. *J. Cell Biology*, 156:715–24, 2002.
- [15] Steven P. Gross, M. Carolina Tuma, Sean W. Deacon, Anna S. Serpinskaya, Amy R. Reilein, and Vladimir I. Gelfand. Interactions and regulation of molecular motors in xenopus melanophores. *Journal of Cell Biology*, 156:85566, 2002.
- [16] Steven P. Gross, Michael A. Welte, Steven M. Block, and Eric F. Wieschaus. Dynein-mediated cargo transport in vivo: A switch controls travel distance. *J. Cell Biol*, 148:945–55, 2000.
- [17] B Guo and WH Guilford. Mechanics of actomyosin bonds in different nucleotide states are tuned to muscle contraction. *PNAS*, 103:9844–49, 2006.
- [18] Adam G. Hendricks, Eran Perlson, Jennifer L. Ross, Harry W. Schroeder III, Mariko Tokito, and Erika L.F. Holzbaur. Motor coordination via a tug-of-war mechanism drives bidirectional vesicle transport. *Current Biology*, 20:697–702, 2010.
- [19] Nobutaka Hirokawa. Kinesin and dynein superfamily proteins, the mechanism of organelle transport. *Science*, 279:519–26, 1998.
- [20] J. Howard, A. J. Hudspeth, and R. D. Vale. Movement of microtubules by single kinesin molecules. *Nature*, 342:154–58, 1989.

- [21] Stephen J. King and Trina A. Schroer. Dynactin increases the processivity of the cytoplasmic dynein motor. *NATURE CELL BIOLOGY*, 2:20–24, 2000.
- [22] Hiroaki Kojima, Etsuko Muto, Hideo Higuchi, and Toshio Yanagida. Mechanics of single kinesin molecules measured by optical trapping nanometry. *Biophysical Journal*, 73:2012–22, 1997.
- [23] Comert Kural, Hwajin Kim, Sheyum Syed, Gohta Goshima, Vladimir I. Gelfand, and Paul R. Selvin. Kinesin and dynein move a peroxisome in vivo: A tug-of-war or coordinated movement? *Science*, 308:1469–72, 2005.
- [24] Kristoffer S. Larsen, Jing Xu, Silvia Cermelli, Zhanyong Shu, and Steven P. Gross. BicaudalD actively regulates microtubule motor activity in lipid droplet transport. *PLoS ONE*, 3, 2008.
- [25] Valeria Levi, Anna S. Serpinskaya, Enrico Gratton, and Vladimir Gelfand. Organelle transport along microtubules in xenopus melanophores: Evidence for cooperation between multiple motors. *Biophysical Journal*, 90:318–27, 2006.
- [26] Roop Mallik, Brian C. Carter, Stephanie A. Lex, Stephen J. King, and Steven P. Gross. Cytoplasmic dynein functions as a gear in response to load. *Nature*, 427:649–52, 2004.

- [27] Roop Mallik, Dmitri Petrov, S.A. Lex, S.J. King, and S.P. Gross. Building complexity: An in vitro study of cytoplasmic dynein with in vivo implications. *Current Biology*, 15:2075–85, 2005.
- [28] Joel E. Martinez, Michael D. Vershinin, George T. Shubeita, and Steven P. Gross. On the use of in vivo cargo velocity as a biophysical marker. *Biochem. and Biophys. Res. Comm.*, 353:835–40, 2007.
- [29] Richard J. McKenney, Michael Vershinin, Ambarish Kunwar, Richard B. Vallee, and Steven P. Gross. Lis1 and nude induce a persistent dynein force-producing state. *Cell*, 141:304–14, 2010.
- [30] M. J. I. Mller, S. Klumpp, and R. Lipowsky. Tug-of-war as a cooperative mechanism for bidirectional cargo transport by molecular motors. *PNAS*, 105:4609 – 14, 2008.
- [31] R.L. Morris and P.J. Hollenbeck. Axonal transport of mitochondria along microtubules and f-actin in living vertebrate neurons. *J. Cell Biol*, 131:131526, 1995.
- [32] Bryce M. Paschal, Howard S. Shpetner, and Richard B. Vallee. Map 1c is a microtubule-activated atpase which translocates microtubules in vitro and has dynein-like properties. *J. of Cell Biology*, 105:1273–82, 1987.
- [33] D.Y. Petrov, R. Mallik, G.T. Shubeita, M. Vershinin, S.P. Gross, and C.C.Yu. Studying molecular motor-based cargo transport: What is real, and what is noise? *Biophys. Journal*, 92:295363, 2007.

- [34] Aaron D. Pilling, Dai Horiuchi, Curtis M. Lively, and William M. Saxton. Kinesin-1 and dynein are the primary motors for fast transport of mitochondria in drosophila motor axons. *Molecular Biology of the Cell*, 17:2057–68, 2006.
- [35] M. Samsó, M. Radermacher, J. Frank, and M.P. Koonce. Structural characterization of a dynein motor domain. *J. Mol. Biol.*, 276:927–37, 1998.
- [36] Trina A. Schroer. Structure, function of dynactin. *Seminars in Cell, Developmental Biology*, 7:321–28, 1996.
- [37] LR Serbus, BJ Cha, WE Theurkauf, and WM Saxton. Dynein and the actin cytoskeleton control kinesin-driven cytoplasmic streaming in drosophila oocytes. *Development*, 132:3743–52, 2005.
- [38] GT Shubeita, SL Tran, J Xu, M Vershinin, S Cermelli, SL Cotton, MA Welte, and SP Gross. Consequences of motor copy number on the intracellular transport of kinesin-1-driven lipid droplets. *Cell*, 135:1098–107, 2008.
- [39] P. A. Sims and X. S. Xie. Probing dynein and kinesin stepping with mechanical manipulation in a living cell. *ChemPhysChem*, 10:1511–16, 2009.
- [40] Virupakshi Soppina, Arpan Kumar Rai, Avin Jayesh Ramaiya, Pradeep Barak, and Roop Mallik. Tug-of-war between dissimilar teams of mi-

- crotubule motors regulates transport and fission of endosomes. *PNAS*, 106:1938186, 2009.
- [41] Ivo A. Telley, Peter Bieling, and Thomas Surrey. Obstacles on the microtubule reduce the processivity of kinesin-1 in a minimal in vitro system and in cell extract. *Biophysical Journal*, 96:3341–3353, 2009.
- [42] Carsten Theissa, Markus Napireib, and Karl Meller. Impairment of anterograde and retrograde neurofilament transport after anti-kinesin and anti-dynein antibody microinjection in chicken dorsal root ganglia. *European Journal of Cell Biology*, 84:29–43, 2005.
- [43] Kurt S. Thorn, Jeffrey A. Ubersax, and Ronald D. Vale. Engineering the processive run length of the kinesin motor. *J. of Cell Biolog*, 151:1093–1100, 2000.
- [44] Shiori Toba, Tomonobu M. Watanabe, Lisa Yamaguchi-Okimoto, Yoko Yano Toyoshima, and Hideo Higuchi. Overlapping hand-over-hand mechanism of single molecular motility of cytoplasmic dynein. *PNAS*, 103:5741–45, 2006.
- [45] Ronald D. Vale. The molecular motor toolbox for intracellular transport. *Cell*, 112:467–80, 2003.
- [46] Ronald D. Vale, Thomas S. Reese, and Michael P. Sheetz. Identification of a novel force-generating protein, kinesin, involved in microtubule-based motility. *Cell*, 42:39 – 50, 1985.

- [47] Michael Vershinin, Brian C. Carter, David S. Razafsky, Stephen J. King, and Steven P. Gross. Multiple-motor based transport and its regulation by tau. *PNAS*, 104:87–92, 2007.
- [48] Koen Visscher, Mark J. Schnitzer, and Steven M. Block. Single kinesin molecules studied with a molecular force clamp. *Nature*, 400:184–89, 1999.
- [49] I Wacker, C Kaether, A Kromer, A Migala, W Almers, and HH Gerdes. Microtubule-dependent transport of secretory vesicles visualized in real time with a GFP-tagged secretory protein. *Journal of Cell Science*, 110:1453–63, 1997.
- [50] R. M. Warn and A. Warn. Microtubule arrays present during the syncytial and cellular blastoderm stages of the early drosophila embryo. *Experimental Cell Research*, 163:201–210, 1986.
- [51] Michael A. Welte, Steven P. Gross, Marya Postner, Steven M. Block, and Eric F. Wieschaus. Developmental regulation of vesicle transport in drosophila embryos: Forces and kinetics. *Cell*, 92:547–57, 2008.
- [52] Ahmet Yildiz, Michio Tomishige, Ronald D. Vale, and Paul R. Selvin. Kinesin walks hand-over-hand. *Science*, 303:676–78, 2004.

Vita

Phil Jack Holzmeister was born in Wertheim, Germany on 06 July 1986, the son of Jürgen Holzmeister and Christiane Holzmeister. After graduating from the Johannes-Butzbach-Gymnasium in Miltenberg in 2005 he fulfilled his 9 month civilian service at the Verein Lebenshilfe Miltenberg eV. Consequently he started studying physics at the Julius-Maximilians-Universität Würzburg in 2006. He passed the Vordiplom in physics in 2008 “sehr gut” (very good) and applied in 2009 for enrollment in the graduate physics program at the University of Texas at Austin as an exchange student. He was accepted and started studies the same year.

Permanent address: Parkring 15
97904 Dorfprozelten
D-Germany

This thesis was typeset with L^AT_EX[†] by the author.

[†]L^AT_EX is a document preparation system developed by Leslie Lamport as a special version of Donald Knuth’s T_EX Program.